Article

Not peer-reviewed version

# Waveguide Polarizers in Silicon with $MoS_2$ Films

David J. Moss *

Posted Date: 30 May 2025

doi: 10.20944/preprints202505.2452.v1

Keywords: integrated photonics; 2D materials; transition metal dichalcogenides; optical polarizers

 doi:10.20944/preprints202505.2452.v1



*Article*

# Waveguide Polarizers in Silicon with $MoS_2$ Films

**David J. Moss**

Swinburne University, Australia; dmoss@swin.edu.au

**Abstract**

Polarization control is of fundamental importance for modern optical systems, and optical polarizers serve as critical components for enabling this functionality. Here, we experimentally demonstrate optical polarizers by integrating 2D molybdenum disulfide ($MoS_2$) films onto silicon photonic waveguides. High-quality monolayer $MoS_2$ films with highly anisotropic light absorption are synthesized via a low-pressure chemical vapor deposition (LPCVD) method and subsequently transferred onto silicon-on-insulator (SOI) nanowire waveguides to fabricate integrated optical polarizers. Detailed measurements are carried out for the fabricated devices with various $MoS_2$ film coating lengths and silicon waveguide geometry. The results show that a maximum polarization-dependent loss of ~21 dB is achieved, together with a high figure of merit of ~4.2. In addition, the hybrid waveguide polarizers exhibit broad operation bandwidth exceeding ~100 nm and excellent power durability. These results highlight the strong potential for on-chip integration of 2D $MoS_2$ films to implement high-performance polarization selective devices.

**Keywords:** integrated photonics; 2D materials; transition metal dichalcogenides; optical polarizers

## 1. Introduction

The control of light polarization plays a crucial role in modern optical systems and underpins a wide range of advanced optical technologies [1,2]. Optical polarizers, which allow transmission of light in a specific polarization while suppressing the orthogonal polarization component, serve as key elements for polarization control in optical systems [3]. To date, a variety of optical polarizers have been developed based on refractive prisms [4,5], birefringent crystals [6,7], fiber components [8,9], and integrated photonic devices [10,11]. However, these polarizers based on bulk materials often struggle to achieve efficient polarization selection over wide wavelength ranges. This limitation is especially significant given the increasing demand for broadband optical polarizers driven by rapid progress in photonic technologies and systems [12,13].

Recently, due to strong anisotropy in light absorption and broadband response, two-dimensional (2D) materials with atomic-scale film thicknesses have been incorporated onto bulk optical waveguides to realize high-performance optical polarizers [14], as demonstrated by those incorporating 2D materials such as graphene [14–16], graphene oxide (GO) [17–19], and transition metal dichalcogenides (TMDCs) [20–22]. As a significant subgroup in the 2D material family, TMDCs exhibit a direct bandgap in their monolayer form that transitions to an indirect bandgap in few-layer or bulk forms [23,24]. This distinctive property facilitates their widespread applications for next-generation atomically thin devices such as transistors [25,26], photodetectors [27,28], and electrocatalysts [29,30]. More recently, the strong anisotropic light absorption of 2D TMDC films across broad wavelength ranges has also been explored, and their integration onto polymer and Neodymium-doped Yttrium Aluminum Garnet (Nd:YAG) waveguides for realizing optical polarizers has been successfully demonstrated [21,22].

In this work, we demonstrate the integration of 2D molybdenum disulfide ($MoS_2$) – a representative TMDC material – onto the widely used silicon photonic platform to realize high-performance optical polarizers. High-quality monolayer $MoS_2$ films with strong anisotropy in light absorption are synthesized via a low-pressure chemical vapor deposition (LPCVD) method, and

 doi:10.20944/preprints202505.2452.v1



subsequently transferred onto silicon-on-insulator (SOI) nanowire waveguides using polymer-assisted transfer process. We perform detailed measurements for the fabricated devices with different $MoS_2$ film coating lengths and silicon waveguide geometry, achieving a maximum polarization-dependent loss of ~21 dB and a high figure of merit of ~4.2. In addition, the hybrid waveguide polarizers exhibit broad operation bandwidth over ~100 nm and excellent power durability. Finally, we compare the performance of our device with state-of-the-art waveguide polarizers incorporating different 2D materials and find that it achieves the highest figure of merit (FOM) among all those based on the silicon photonic platform. These results reveal the strong potential of 2D TMDC films for implementing high-performance integrated polarization selective devices.

## 2. Device Design

As an important member of the TMDCs family that has been widely studied, $MoS_2$ features a hexagonal sheet of molybdenum (Mo) atoms sandwiched between two hexagonal sheets of sulfur (S) atoms [31,32]. Figure 1(a) illustrates the atomic structure of monolayer $MoS_2$, where Mo and S atoms are connected by strong covalent bonds. Multi-layered $MoS_2$ consists of vertically stacked layers that are weakly bonded through van der Waals interactions [26]. Monolayer $MoS_2$ has shown great potential as a semiconducting material with a direct bandgap of ~1.8 – 1.9 eV [33]. This is larger than the energy of two photons at 1550 nm (i.e., ~1.6 eV), which allows for relatively low linear light absorption as well as two-photon absorption at near infrared wavelengths. The quality of 2D $MoS_2$ crystals plays a crucial role in determining the material properties such as refractive index, light absorption, and optical bandgap, which correlates to the intrinsic structural defects induced by sulfur vacancies [34,35]. In this work, we choose $MoS_2$ to implement optical polarizers due to several compelling advantages. First, it exhibits strong anisotropic light absorption over a very broad spectral bandwidth [36,37]. Second, it possesses relatively low linear absorption in the infrared regime, with an extinction coefficient nearly 1 order of magnitude lower than that of graphene [38,39], making it particularly suitable for infrared photonic applications. Finally, we develop a simple and one-step chemical vapor deposition (CVD) method to fabricate $MoS_2$ films with precise control over structural defects [34], which allows us to tailor the intrinsic optical properties of $MoS_2$ for specific optical applications.

Figure 1(b) shows the schematic of an integrated waveguide polarizer consisting of a silicon nanowire waveguide coated with a monolayer $MoS_2$ film. Similar to other 2D materials such as graphene and graphene oxide (GO) [14,15,17,19], 2D $MoS_2$ films exhibit strong anisotropic optical absorption [40,41], with significantly higher absorption for light propagating in the in-plane direction compared to the out-of-plane direction. For the hybrid waveguide in Figure 1(b), these directions correspond to TE- and TM-polarized incident light, respectively. As a result, the hybrid waveguide can effectively operate as a TM-pass waveguide polarizer. It is worth noting that 2D $MoS_2$ exhibits a broad spectral range of material anisotropy spanning from visible to infrared wavelengths [36]. This wide bandwidth offers a significant advantage for $MoS_2$-coated integrated waveguide polarizers, which is difficult to achieve for conventional bulk silicon photonic polarizers [1,14,42].

Figure 1(c) shows a schematic of the cross section of the hybrid waveguide in Figure 1(b). The corresponding transverse electric (TE) and transverse magnetic (TM) mode profiles at 1550 nm are provided in Figure 1(d), which were simulated using commercial mode-solving software (COMSOL Multiphysics). In our simulation, the thickness of the monolayer $MoS_2$ film was ~0.7 nm. The refractive index ($n$) and extinction coefficient ($k$) of $MoS_2$ for TE polarization were $n_{TE}$ = ~3.8 and $k_{TE}$ = ~0.107, respectively. For TM polarization, the corresponding values were $n_{TM}$ = ~3.2 and $k_{TM}$ = ~0.027. These values were obtained from our measurements in the following sections. The simulated TE- and TM polarized effective indices for the hybrid waveguide were ~2.081 + 3.313 × $10^{-4}$i and ~1.551 + 7.132 × $10^{-5}$i, respectively. The large difference in the imaginary part highlights the polarization selectivity for the hybrid waveguide, which originates from the significant disparity between $k_{TE}$ and $k_{TM}$ of the 2D $MoS_2$ film. It should be noted that, due to the polymer-assisted transfer method used in our fabrication process (which will be discussed in Section 3), the monolayer $MoS_2$ film does not

 doi:10.20944/preprints202505.2452.v1



conformally coat on the sidewalls of the silicon nanowire waveguide, resulting in air gaps between the waveguide sidewalls and the $MoS_2$ film. Nevertheless, this has minimal impact on the polarization selectivity of the hybrid waveguides, as it mainly depends on the interaction between the evanescent field and the $MoS_2$ film on the waveguide top surface.

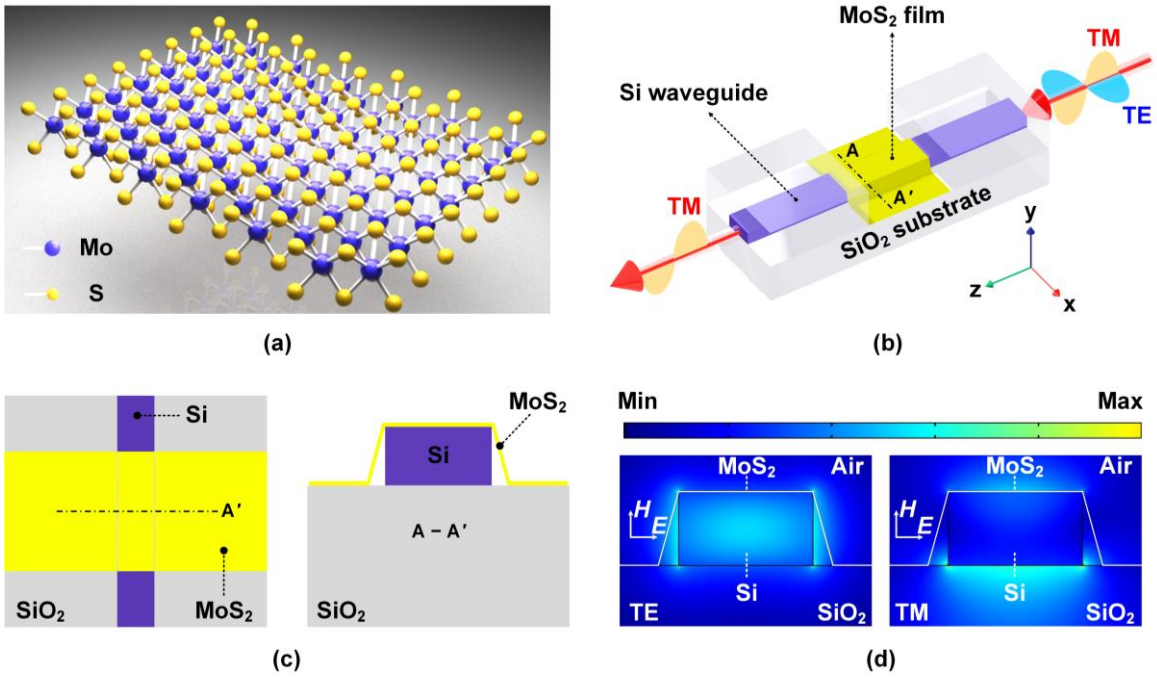


**Figure 1.** (**a**) Schematic atomic structure of monolayer molybdenum disulfide ($MoS_2$). (**b**) Schematic illustration of a silicon (Si) nanowire waveguide integrated with a monolayer $MoS_2$ film as a waveguide polarizer. (**c**) Schematic illustrations of top view and cross section of the hybrid waveguide in (**b**). (**d**) TE and TM mode profiles for the hybrid waveguide in (**c**).

## 3. Device Fabrication and Material Characterization

Based on the device design in Section **2**, we fabricated silicon photonic waveguide polarizers coated with monolayer $MoS_2$ films in this section. In addition, we employed a range of material characterization methods to assess the quality of the $MoS_2$ films on the photonic integrated chips.

We first fabricated uncoated silicon nanowire waveguides using CMOS-compatible fabrication technologies. The nanowire waveguides were fabricated on silicon-on-insulator (SOI) wafer with a 220-nm-thick top silicon layer and a 2-μm-thick silica layer. The waveguide patterns were defined using 248-nm deep ultraviolet photolithography, followed by waveguide formation through an inductively coupled plasma etching process. After this, a 1.5-μm-thick silica layer serving as an upper cladding layer was deposited on the SOI chip via plasma enhanced chemical vapor deposition (PECVD). Finally, windows of different lengths were opened on the silica upper cladding through the processes of photolithography and reactive ion etching (RIE) to enable the coating of $MoS_2$ films onto the silicon waveguides. All the nanowire waveguides we fabricated had the same length of ~3.0 mm, and the lengths of the opened windows (i.e., the $MoS_2$ film coating lengths) ranged between ~0.1 mm and ~2.2 mm.

After fabricating the uncoated silicon waveguides, we used an LPCVD method that we developed in Ref. [34] to synthesize high-quality $MoS_2$ films. Our method allows for precise control of the intrinsic atomic defects induced by sulfur vacancies, and supports the direct growth of high-quality and large-area 2D $MoS_2$ films with precise thickness control. Figure 2(a) shows a schematic of our CVD process flow using a two-temperature-zone tube furnace to synthesize $MoS_2$ monolayers. First, the Mo precursor was drop-casted onto an ultrasonically cleaned substrate in Zone 2 of the furnace, which was maintained at 750 °C during the CVD process. After this, S powder was vaporized

 doi:10.20944/preprints202505.2452.v1



at 180 °C in Zone 1, and the S vapors were carried downstream by a 70 sccm flow of argon as carrier gas into Zone 2. Finally, a surface reaction between the Mo and S species occurred, resulting in the synthesis of $MoS_2$ single crystals. During the growth, the process pressure was maintained at ~1 torr to maintain a low-pressure CVD conditions. Figure 2(b) shows a microscopic image of a monolayer $MoS_2$ film grown on a sapphire substrate, which exhibits a high film uniformity. Figure 2(c) shows an atomic force microscopy (AFM) image of a representative $MoS_2$ crystal synthesized by using our CVD method, which shows an average thickness of ~0.7 nm.

Following the CVD synthesis of a monolayer $MoS_2$ film, it was transferred onto the SOI chip with uncoated silicon waveguides using a polymer-assisted transfer process [43]. The as-grown $MoS_2$ film was initially spin-coated with a polystyrene (PS) support layer. Subsequently, the PS/$MoS_2$ stack was exfoliated from the growth substrate using a water-droplet-assisted delamination process, driven by surface energy differences between the interfaces [44]. Finally, the resulting stack was then stamped onto the SOI chip via van der Waals interactions, and the PS layer was removed by dissolving it in toluene. As shown in Figure 2(d), the transferred monolayer $MoS_2$ film exhibits high optical transmittance and uniform coverage across the SOI chip surface, confirming the effectiveness and quality of the transfer process.

Figure 3(a-i) and (a-ii) show the Raman spectra of the same SOI chip before and after the transfer of monolayer $MoS_2$ film, which were measured by using a ~514-nm excitation laser. After $MoS_2$ integration, the Raman spectrum exhibits two prominent peaks emerging at ~384 $cm^{-1}$ and ~404 $cm^{-1}$, corresponding to the in-plane ($E^1_{2g}$) TE and out-of-plane ($A_{1g}$) TM vibrational modes of monolayer $MoS_2$, respectively. Moreover, the observed frequency difference of ~20 $cm^{-1}$ is characteristic of monolayer $MoS_2$. An additional peak observed at ~517 $cm^{-1}$ originates from the underlying silicon substrate. These spectral features are consistent with those reported previously for CVD-grown monolayer $MoS_2$ [34,45,46], confirming successful and high-quality integration of 2D $MoS_2$ onto the SOI chip.

Figure 3(b) shows the spectra for linear optical absorption and transmittance of the synthesized $MoS_2$ film, which were characterized via ultraviolet–visible (UV–vis) spectrometry. It can be seen that the $MoS_2$ exhibited strong light absorption in the visible and infrared wavelength regions. The linear absorption spectrum exhibited a sharp increase followed by a rapid decline within the range of ~400 – 600 nm. Two strong absorption peaks were observed at ~605 $cm^{-1}$ and ~651 $cm^{-1}$, and the peak associated with van Hove singularities [47] of monolayer $MoS_2$ was also observed at ~430 $cm^{-1}$. Before a gradual decrease at wavelengths >900 nm, the linear absorption spectrum exhibited a sudden jump at ~870 nm. The transmittance of the sample had a transmittance >60% at wavelengths between ~400 nm and ~1800 nm. These results show agreement with those reported in previous studies [48–50] and further validate the high quality of our synthesized 2D $MoS_2$ films.

Figure 3(c) shows the X-ray diffraction (XRD) spectrum for the synthesized $MoS_2$ film. The diffraction rings can be indexed to the (100), (103), (105), and (110) reflections of hexagonal $MoS_2$ crystal structure, which shows an agreement with the measured XRD spectra of $MoS_2$ in Refs. [51,52]. Figure 3(d) shows the X-ray photoelectron spectroscopy (XPS) analysis of the synthesized $MoS_2$ film. In Figure 3(d-i), prominent peaks were observed at ~226.9 eV, ~229.6 eV, and ~232.7 eV, which correspond to S 2*s*, Mo 3*d* doublet of $Mo^{4+}$ $3d_{5/2}$ and $Mo^{4+}$ $3d_{3/2}$. In addition, weak peaks at ~232.3 eV and ~235.4 eV were attributed to the $3d_{5/2}$ and $3d_{3/2}$ components of $Mo^{6+}$, indicating the presence of $MoO_x$ species, likely originating from partial surface oxidation or physiosorbed oxygen during ambient exposure [35]. Figure 3(d-ii) displays the *S 2p* region, where two peaks appeared at ~162.6 eV and ~163.8 eV and corresponded to the S $2p_{3/2}$ and S $2p_{1/2}$, respectively, further supporting the formation of $MoS_2$ with the expected stoichiometry. These experimental results are consistent with previously reported XPS signatures of CVD-grown monolayer $MoS_2$ in Refs. [46,53–55].

 doi:10.20944/preprints202505.2452.v1



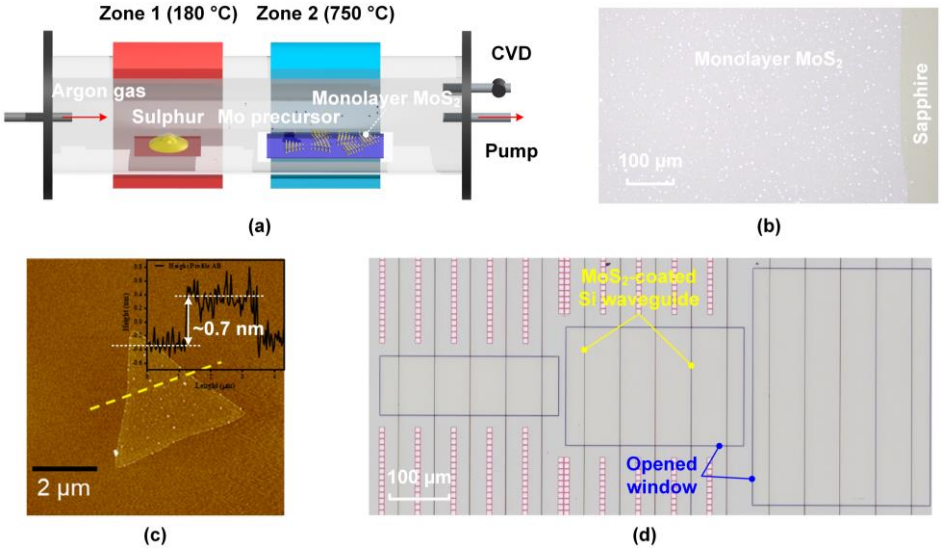


**Figure 2.** (**a**) Schematic illustration showing the chemical vapor deposition (CVD) process flow we employed for synthesizing $MoS_2$ monolayers. (**b**) Microscopic image of a monolayer $MoS_2$ film coated on a sapphire substrate. (**c**) Atomic force microscopy (AFM) image of a $MoS_2$ crystal synthesized by using the CVD method in (**a**). (**d**) Microscopic image of a $MoS_2$-coated silicon-on-insulator (SOI) chip with opened windows.

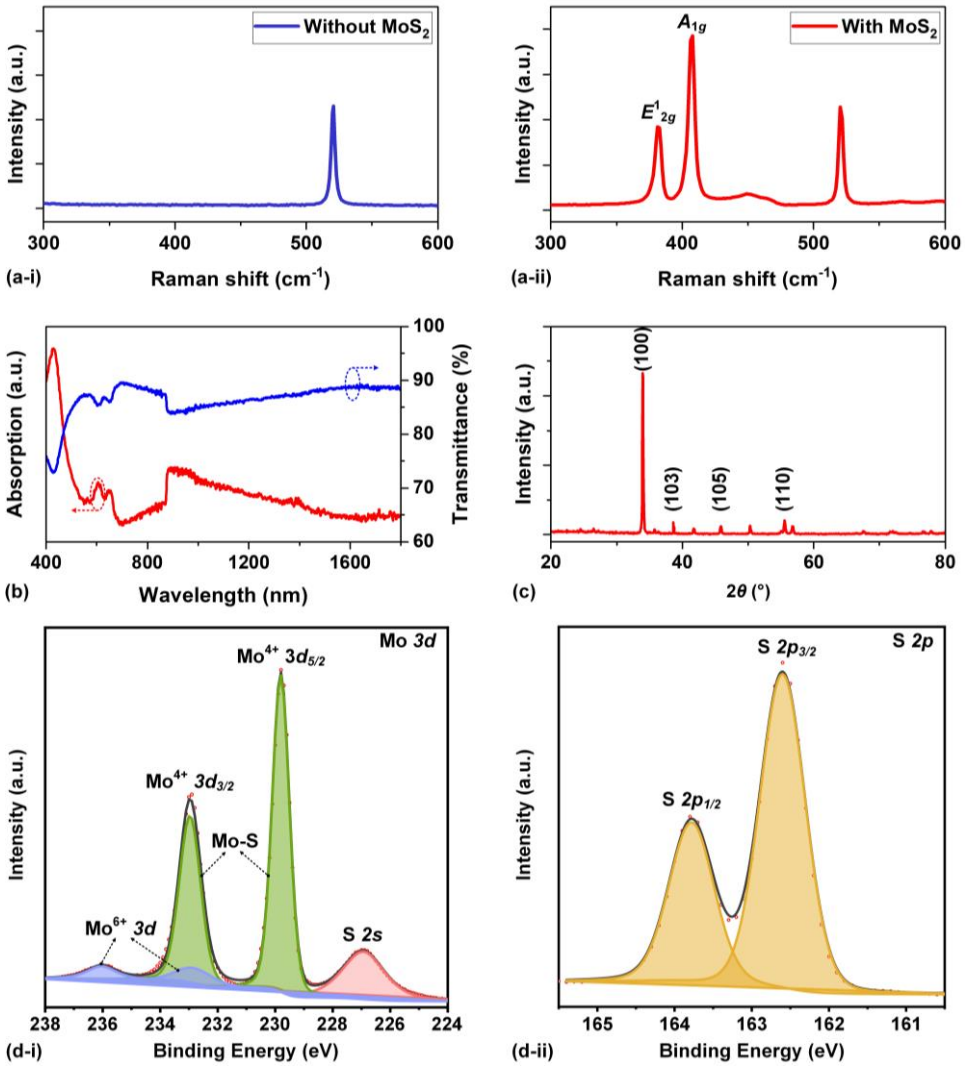

 doi:10.20944/preprints202505.2452.v1



**Figure 3.** Characterization of our synthesized monolayer $MoS_2$ films. (**a**) Measured Raman spectra of an SOI chip (**i**) before and (**ii**) after coating a monolayer $MoS_2$ film. (**b**) Ultraviolet–visible (UV–vis) absorption and transmittance spectra. (c) X-ray diffraction (XRD) spectrum. (**d**) X-ray photoelectron spectroscopy (XPS) spectra, where (**i**) and (**ii**) show characteristic peaks of Mo 3*d* and S 2*p*, respectively.

## 4. Polarization-Dependent Loss Measurements

In this section, we measured the polarization-dependent loss (*PDL*) of the fabricated $MoS_2$-Si hybrid waveguides in Section 3 for input continuous-wave (CW) light with different polarization states. We performed measurements for devices with various silicon waveguide widths ($W$) and with monolayer $MoS_2$ films of different coating lengths ($L_c$). In our measurements, lensed fibers were employed to butt couple a CW light at ~1550 nm into and out of the fabricated devices with inverse-taper couplers at both ends. The fiber-to-chip coupling loss was ~5 dB / facet.

Figure 4(a-i) plot the measured TE- and TM-polarized insertion loss (*IL*) versus $MoS_2$ film coating length $L_c$ for the hybrid waveguides with monolayer $MoS_2$ films. For comparison, all the devices had the same $W$ = ~400 nm. During our measurements in Figure 4, the input CW power and wavelength were kept the same as $P_{in}$ = ~0 dBm and $\lambda$ = ~1550 nm, respectively. Unless otherwise specified, the values of $P_{in}$ and *IL* in our following discussions refer to those after excluding the fiber-to-chip coupling loss.

In Figure 4(a-i), the data points depict the average of measurements on three duplicate devices, and the error bars reflect the variations among different devices. As can be seen, the *IL* increases with $L_c$ for both TE and TM polarizations, with the former exhibiting a faster rate of increase than the latter. This reflects a higher propagation loss for TE polarization, which is associated with a larger imaginary part of its effective index, as simulated in Figure 1(d).

In Figure 4(a-ii), we further calculated the *PDL* (dB) by subtracting the TM-polarized *IL* from the TE-polarized *IL* in Figure 4(a-i). For the device with $L_c$ = 2.2 mm, a maximum *PDL* value of ~21 dB was achieved. In contrast, the uncoated Si waveguide did not show any significant polarization-dependent *IL*, with a *PDL* below 0.5 dB. The huge difference in the *PDL* values highlights the polarization selectivity introduced by integrating a 2D $MoS_2$ film onto the silicon photonic waveguide. In Figure 4(a-i), the *PDL* increases with $L_c$, this further confirms that the exceptional polarization selectivity arises from the 2D $MoS_2$ film and suggests that improved *PDL* can be achieved by increasing the $MoS_2$ film coating length.

Figure 4(b-i) shows the measured TE- and TM-polarized *IL* versus waveguide width $W$ for the hybrid waveguides with the same $L_c$ = ~2.2 mm. In Figure 4(b-i), the *IL* increases with $W$ for TM polarization but decreases for TE polarization. This is mainly resulting from changes in the mode overlap of TE and TM modes induced by variations in the silicon waveguide width. Figure 4(b-ii) shows the corresponding *PDL* calculated from the measured *IL* in Figure 4(b-i). The device with $W$ = ~400 nm achieved a maximum *PDL* of ~21 dB, and the *PDL* decreased as $W$ increased, reaching ~15 dB at $W$ = ~600 nm. Figure 4(c) shows the polar diagrams for the measured *IL* of devices with the same $W$ = ~400 nm but different $L_c$ = ~1.0 mm and ~2.2 mm. In the polar diagrams, the variations in the *IL* values across different polarization angles further confirm the polarization selectivity of the $MoS_2$-Si hybrid waveguides.

In addition to measuring *PDL* at constant wavelength ($\lambda$ = ~1550 nm) and power ($P_{in}$ = ~0 dBm) for the input CW light in Figure 4, we also investigated the dependence of the *PDL* on input light wavelength and power. Figure 5(a) shows the measured *PDL* versus input CW wavelength $\lambda$ for the hybrid waveguides with various $L_c$ but the same $W$ = 400 nm. During our measurements, the input CW power was maintained at $P_{in}$ = ~0 dBm. For all the devices, there were no obvious changes in the *PDL* (< 2 dB) within the measured wavelength range of ~1500 – 1600 nm. We also notice that there was a minor increase in the *PDL* as $\lambda$ increased, which can be attributed to a slight change in $MoS_2$'s mode overlap induced by dispersion. Figure 5(b) shows the measured *PDL* versus $\lambda$ for the hybrid waveguides with various $W$ but the same $L_c$ = ~2.2 mm. Similarly, there were no significant variations in the *PDL*, with only a slight increase in the *PDL* as $\lambda$ increased.

 doi:10.20944/preprints202505.2452.v1



The results in Figure 5(a) and (b) highlight the broadband operation of the $MoS_2$-Si waveguide polarizers – a feature that is often challenging to achieve for bulk silicon photonic polarizers [3,56]. In our measurements, the wavelength tuning range was limited by the tunable CW laser employed to scan the transmission spectra. In fact, $MoS_2$ films exhibit a broad bandwidth for anisotropic light absorption, which extends well beyond that demonstrated here and can span from the visible to the infrared wavelength regions [36,37].

Figure 5(c) and (d) show the measured TE- and TM-polarized *IL* and calculated *PDL* versus input CW power $P_{in}$ for the hybrid waveguides with the same $W$ = ~400 nm but different $L_c$ = ~1.0 mm and ~2.2 mm, respectively. For comparison, the input CW wavelength was kept the same at $\lambda$ = ~1550 nm. In both figures, there are no notable changes in the *IL* and *PDL* within the input power range of ~0 dBm – ~28 dBm. This indicates excellent thermal stability of the 2D $MoS_2$ films and remarkable power durability of the hybrid devices. In contrast, 2D GO films coated on silicon waveguides are susceptible to photothermal reduction at $P_{in}$ > 10 dBm, as observed in our previous measurements [57]. We did not perform measurements for $P_{in}$ > ~28 dBm, as $P_{in}$ = ~28 dBm was the maximum available from our experimental setup. This value accounts for a 5-dB coupling loss subtracted from the 33-dBm maximum CW power, which was achieved after amplification by an erbium-doped fiber amplifier (EDFA).

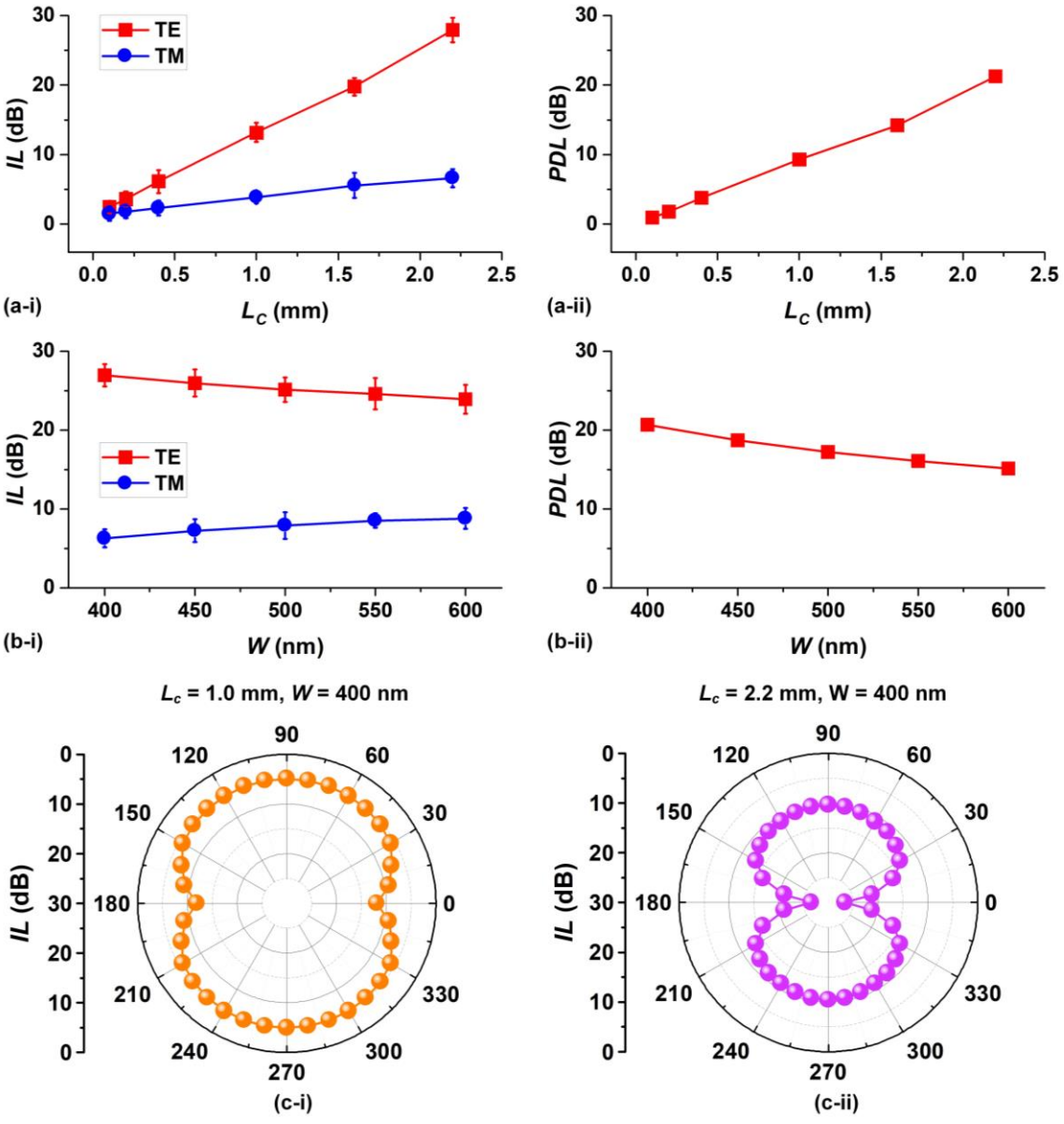

 doi:10.20944/preprints202505.2452.v1



**Figure 4.** (**a**) Measured *IL* versus $MoS_2$ film coating length ($L_c$) for the $MoS_2$-Si hybrid waveguides. (**b**) Measured insertion loss (*IL*) versus the waveguide width (*W*) for the $MoS_2$-Si hybrid waveguides. In (**a**) and (**b**), (**i**) shows the measured results for TE & TM polarizations, and (**ii**) shows the polarization dependent loss (*PDL*) calculated from (**i**). (**c**) Polar diagrams for the measured *IL* of devices with (**i**) $L_c$ = 1.0 mm and (**ii**) $L_c$ = 2.2 mm. The polar angle represents the angle between the input polarization plane and the substrate. In (**a-c**), the input continuous-wave (CW) power and wavelength were $P_{in}$ = ~0 dBm and $\lambda$ = ~1550 nm, respectively. In (**c**), *W* = ~400 nm.

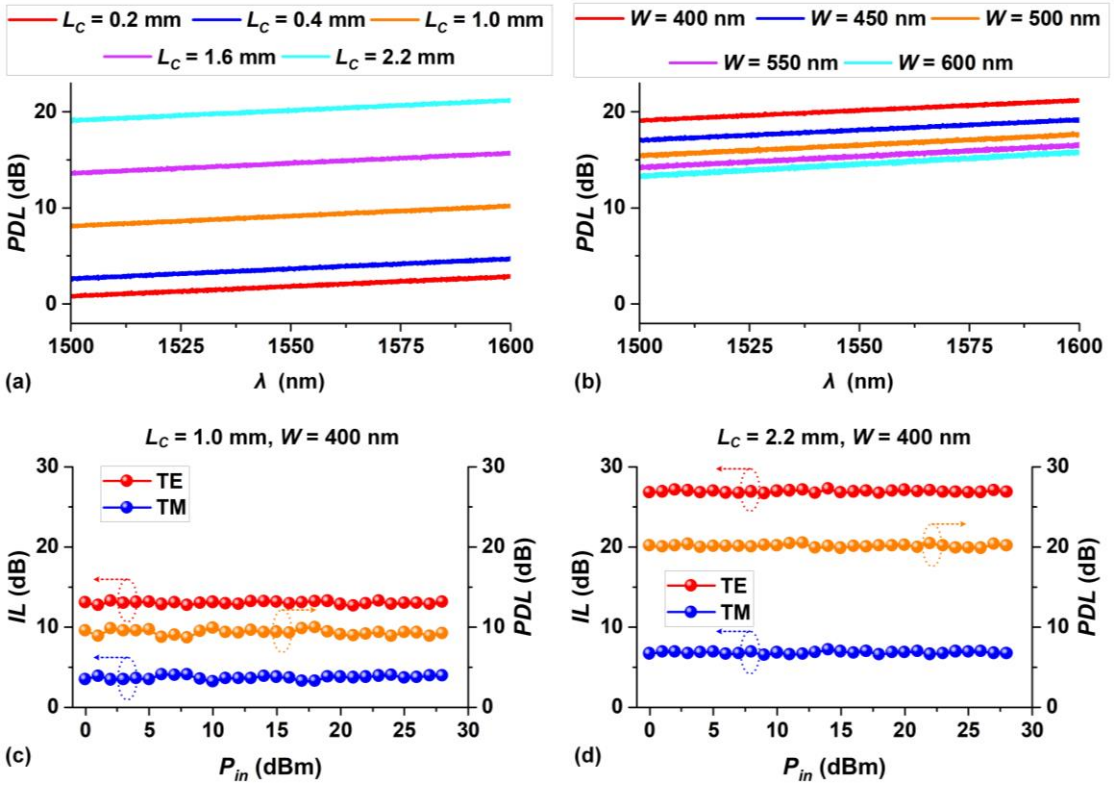


**Figure 5.** (**a**) Measured *PDL* versus input CW wavelength $\lambda$ for the $MoS_2$-Si hybrid waveguides with different $L_c$ but the same *W* of ~400 nm. (**b**) Measured *PDL* versus $\lambda$ for the $MoS_2$-Si hybrid waveguides with different *W* but the same $L_c$ of ~2.2 mm. (**c**) – (**d**) Measured TE- and TM-polarized *IL* and calculated *PDL* versus input power $P_{in}$ for the $MoS_2$-Si hybrid waveguides with $L_c$ = ~1.0 mm and ~2.2 mm, respectively. In (**a**) and (**b**), $P_{in}$ = ~0 dBm. In (**c**) and (**d**), the input CW wavelength and the waveguide width were $\lambda$ = ~1550 nm and *W* = ~400 nm, respectively.

## 5. Discussion

In this section, we further analyze the anisotropic absorption of 2D $MoS_2$ films by fitting the experimental results in Section 4 with theoretical simulations. We also compare the performance of our $MoS_2$-Si waveguide polarizers with waveguide polarizers incorporating other 2D materials.

Figure 6(a) shows the waveguide propagation loss (*PL*) versus *W* for both TE and TM polarizations, which was extracted from the measured *IL* in Figure 4(b). As expected, the TE-polarized *PL* is much higher than the corresponding TM-polarized *PL*. An increase in *W* leads to a smaller difference between the two, mainly caused by altered mode overlap with the $MoS_2$ films. The excess propagation loss (*EPL*) induced by the $MoS_2$ film was further calculated by excluding the *PL* for the uncoated silicon waveguide, which were ~3.4 dB/cm and ~3.0 dB/cm for TE and TM polarizations, respectively. At *W* = 400 nm, the TE-polarized *EPL* was ~117 dB/cm, significantly higher than the TM-polarized *EPL* of ~25 dB/cm, showing agreement with those reported in Ref. [58]. We also note that the value of ~117 dB/cm is more than an order of magnitude lower than the *EPL* induced

 doi:10.20944/preprints202505.2452.v1



by monolayer graphene coated on a silicon waveguide (i.e., ~2000 dB/cm [39,59]), yet ~5 times higher than that induced by monolayer GO (i.e., ~20 dB/cm [60]).

Figure 6(b) shows the extinction coefficient of $MoS_2$ ($k_{TE}$, $k_{TM}$ for TE and TM polarizations, respectively) obtained by fitting the results in Figure 6(a) with optical mode simulations of the hybrid waveguides (at 1550 nm). At $W$ = ~400 nm, $k_{TE}$ is ~0.107, which is about ~4 times that of $k_{TM}$. For all different $W$, the $k$ values for TE polarization are significantly higher than those for TM polarization, highlighting the strong anisotropic light absorption of 2D $MoS_2$ films. For both polarizations, no significant variations in $k$ were observed as $W$ increased. This indicates that the changes in $PL$ with $W$ observed in Figure 6(a) are mainly caused by variations in mode overlap, rather than differences in the $MoS_2$ film properties, highlighting the consistency of our measurements and uniformity of the coated $MoS_2$ film.

In Figure 6(c), we further plot the anisotropy ratios defined as the ratios of the corresponding $k$ values for TE and TM polarizations ($k_{TE}$ / $k_{TM}$) in Figure 6(b). As can be seen, the anisotropy ratio also remained relatively consistent without any significant variations. A maximum anisotropy ratio of ~4.0 is achieved for monolayer $MoS_2$ films, which is close to ~4.5 reported for monolayer GO films [18].

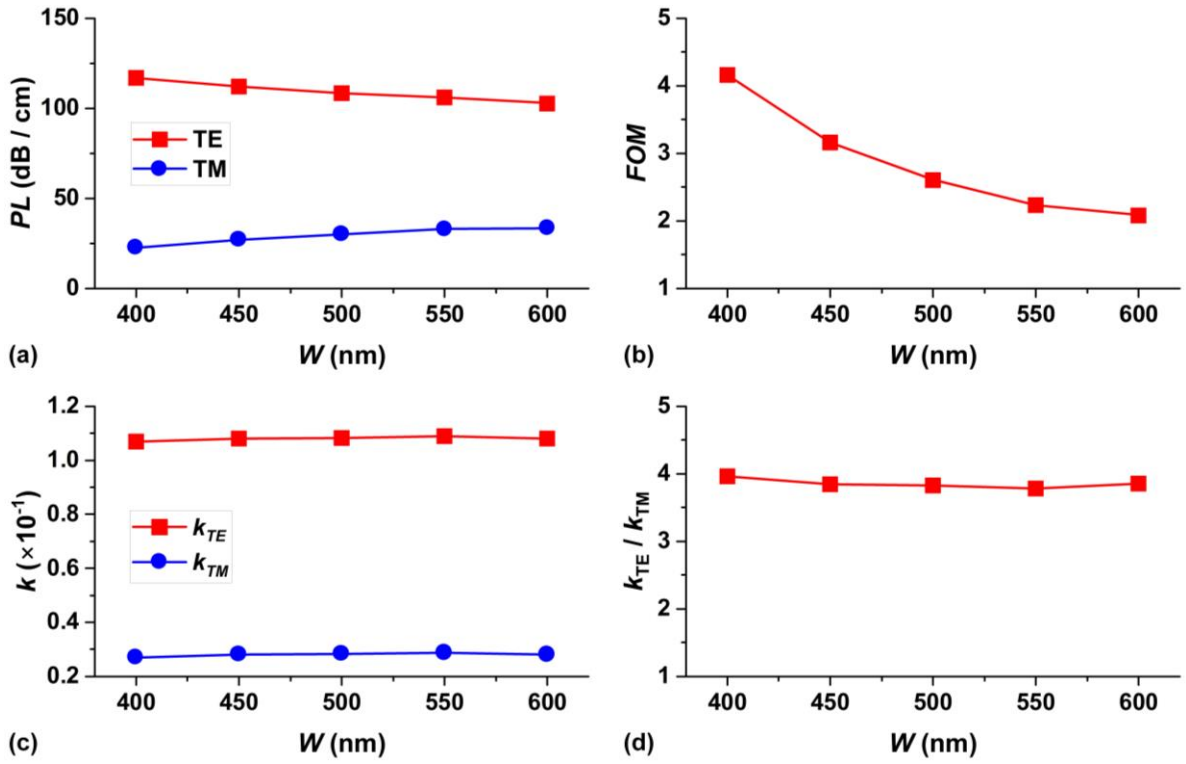


**Figure 6.** (**a**) TE- and TM-polarized propagation loss ($PL$) versus silicon waveguide width $W$ for the $MoS_2$-Si hybrid waveguides. (**b**) TE- and TM-polarized extinction coefficients of $MoS_2$ ($k_{TE}$ , $k_{TM}$) versus $W$ obtained by fitting the results in (**a**) with optical mode simulations. (**c**) Anisotropy ratio ($k_{TE}$ / $k_{TM}$) calculated from (**b**). (**d**) Calculated figures of merit ($FOM$) versus $W$ for the $MoS_2$-Si hybrid waveguides.

To evaluate the performance of 2D-material-based optical polarizers, the figure of merit ($FOM$), defined by the following equation, is commonly used [14,17],

$$FOM = PDL / EIL \quad (1)$$

where $PDL$ (dB) is the ratio of the maximum to minimum $IL$'s as we discussed in Figure 4(a-ii) and (b-ii), and $EIL$ (dB) is the minimum insertion loss induced by the $MoS_2$ film over the uncoated waveguide. Note that the $EIL$ accounts only for the $IL$ induced by the $MoS_2$ film. In our case, it

 doi:10.20944/preprints202505.2452.v1



represents the excess $MoS_2$-induced *IL* for the TM polarization, as the TM mode exhibited a lower *IL*. Figure 6(d) shows the calculated *FOM* versus silicon waveguide width *W*. A higher *FOM* value is achieved for a lower *W*. A maximum *FOM* of ~4.2 was achieved at *W* = ~400 nm, which decreased to ~2.0 as *W* increased to ~600 nm.

In Table 1, we summarize state-of-the-art waveguide optical polarizers incorporating 2D materials and compare their performance. Here we only show the results for experimental works, and compare the key performance parameters including *PDL*, operation bandwidth (*OBW*), and *FOM*. Among the different polarizers, our work here marks the first demonstration of implementing optical polarizers by integrating 2D $MoS_2$ films onto silicon photonic devices. Although other studies have reported higher *FOM* values using waveguides with larger cross-sections [61], thicker 2D materials [19], or enhanced mode overlap [14], it is important to highlight that our device achieves the highest *FOM* among all polarizers implemented based on the silicon photonic platform, which remains the most widely used and influential integrated photonics platform [63–65]. It is also worth noting that there remains substantial room to improve the *FOM* of $MoS_2$-Si hybrid waveguides by tailoring waveguide geometry to optimize mode overlap. Simulations show that a *FOM* value of ~19.2 can be achieved for a hybrid device with a cross-section of 400 nm × 160 nm for the bare silicon waveguide.

**Table 1.** Comparison of waveguide optical polarizers incorporating 2D materials.

| 2D Material | Waveguide Material | 2D Material Thickness | WD (μm) | *PDL (dB)* | OBW (μm) | *FOM* | Ref. |
|---|---|---|---|---|---|---|---|
| Graphene | Polymer | – [a] | 7.00 × 5.00 | ~19 | – [a] | ~0.7 | [16] |
| Graphene | Glass | – [a] | 11.50 × 2.60 | ~27 | ~1.23–1.61 | ~3.0 | [61] |
| Graphene | Chalcogenide | Monolayer | – [a] | ~23 | ~0.94–1.60 | ~28.8 | [14] |
| Graphene | Polymer | > or < 10 nm [b] | 10.00 × 5.00 | ~6 | – [a] | ~0.7 | [15] |
| $MoS_2$ | Nd:YAG | ~6.5 nm | – [a] | ~3 | – [a] | ~7.5 | [21] |
| $MoS_2$ | Polymer | ~2.5 nm | 8.00 × 8.00 | ~12.6 | ~0.65–0.98 | – [a] | [22] |
| GO | Polymer | ~2000 nm | 10.00 × 5.00 | ~40 | ~1.53–1.63 | ~6.2 | [19] |
| GO | Doped silica | ~2–200 nm | 3.00 × 2.00 | ~54 | ~0.63–1.60 | ~7.2 | [17] |
| GO | Silicon | ~10 nm | 0.40 × 0.22 | ~17 | ~1.50–1.60 | ~1.7 | [18] |
| rGO | Silicon | Monolayer | 0.40 × 0.22 | ~47 | ~1.50–1.60 | ~3.0 | [62] |
| $MoS_2$ | Silicon | Monolayer | 0.40 × 0.22 | ~21 | ~1.50–1.60 | ~4.2 | This work |

*WD*: waveguide dimension, *PDL*: polarization dependent loss, *OBW*: operational bandwidth, *IL*: insertion loss, *FOM*: figure of merit. [a]There is no reported value for this parameter in the literature. [b]The polymer waveguides with a few-layer graphene film (< 10 nm) and a thicker graphene film (> 10 nm) worked as TM- and TE-pass optical polarizers, respectively.

These results confirm the effectiveness of integrating 2D GO films onto silicon photonic platforms to implement high-performance thermo-optic devices and will have implications for a wide range of devices such as optical microcombs, [65–145] advanced circuits, [146–153] graphene oxide and other 2D material based devices, [154–191] and quantum optics. [192–207]

## 6. Concluson

In summary, we integrate 2D $MoS_2$ films onto SOI nanowire waveguides to implement high-performance optical polarizers. High-quality monolayer $MoS_2$ films exhibiting highly anisotropic light absorption are synthesized via a LPCVD method, and then transferred onto SOI nanowire waveguides using a polymer-assisted transfer process. Detailed measurements are performed for our fabricated devices with various $MoS_2$ film coating lengths and silicon waveguide geometry. The results show that a maximum *PDL* of ~21 dB and a high *FOM* of ~4.2 are achieved. The hybrid waveguide polarizers also demonstrate a broad operation bandwidth of over ~100 nm and excellent

 doi:10.20944/preprints202505.2452.v1



power durability. These results verify the effectiveness of integrating 2D $MoS_2$ films onto silicon photonic devices for implementing high-performance optical polarizers.

## References


1. Q. Bao, H. Zhang, B. Wang, Z. Ni, C. H. Y. X. Lim, Y. Wang, D. Y. Tang, and K. P. Loh, "Broadband graphene polarizer," *Nature Photonics,* vol. 5, no. 7, pp. 411-415, 2011/07/01, 2011.
2. Y. Yan, G. Xie, M. P. J. Lavery, H. Huang, N. Ahmed, C. Bao, Y. Ren, Y. Cao, L. Li, Z. Zhao, A. F. Molisch, M. Tur, M. J. Padgett, and A. E. Willner, "High-capacity millimetre-wave communications with orbital angular momentum multiplexing," *Nature Communications,* vol. 5, no. 1, pp. 4876, 2014/09/16, 2014.
3. D. Dai, L. Liu, S. Gao, D.-X. Xu, and S. He, "Polarization management for silicon photonic integrated circuits," *Laser & Photonics Reviews,* vol. 7, no. 3, pp. 303-328, 2013.
4. K. Serkowski, D. S. Mathewson, and V. L. Ford, "Wavelength dependence of interstellar polarization and ratio of total to selective extinction," *The Astrophysical Journal,* vol. 196, pp. 261-290, February 01, 1975, 1975.
5. T. J. Wang, Q. Y. He, J. Y. Gao, Y. Jiang, Z. H. Kang, H. Sun, L. S. Yu, X. F. Yuan, and J. Wu, "Efficient electrooptically Q-switched Er:Cr:YSGG laser oscillator-amplifier system with a Glan-Taylor prism polarizer," *Laser Physics,* vol. 16, no. 12, pp. 1605-1609, 2006/12/01, 2006.
6. E. Saitoh, Y. Kawaguchi, K. Saitoh, and M. Koshiba, "TE/TM-Pass Polarizer Based on Lithium Niobate on Insulator Ridge Waveguide," *IEEE Photonics Journal,* vol. 5, no. 2, pp. 6600610-6600610, 2013.
7. A. Rahnama, T. Dadalyan, K. Mahmoud Aghdami, T. Galstian, and P. R. Herman, "In-Fiber Switchable Polarization Filter Based on Liquid Crystal Filled Hollow-Filament Bragg Gratings," *Advanced Optical Materials,* vol. 9, no. 19, pp. 2100054, 2021.
8. J. Wang, J.-Y. Yang, I. M. Fazal, N. Ahmed, Y. Yan, H. Huang, Y. Ren, Y. Yue, S. Dolinar, M. Tur, and A. E. Willner, "Terabit free-space data transmission employing orbital angular momentum multiplexing," *Nature Photonics,* vol. 6, no. 7, pp. 488-496, 2012/07/01, 2012.
9. N. Bozinovic, Y. Yue, Y. Ren, M. Tur, P. Kristensen, H. Huang, A. E. Willner, and S. Ramachandran, "Terabit-Scale Orbital Angular Momentum Mode Division Multiplexing in Fibers," *Science,* vol. 340, no. 6140, pp. 1545-1548, 2013.
10. D. Dai, Z. Wang, N. Julian, and J. E. Bowers, "Compact broadband polarizer based on shallowly-etched silicon-on-insulator ridge optical waveguides," *Optics Express,* vol. 18, no. 26, pp. 27404-27415, 2010/12/20, 2010.
11. Y. Huang, S. Zhu, H. Zhang, T.-Y. Liow, and G.-Q. Lo, "CMOS compatible horizontal nanoplasmonic slot waveguides TE-pass polarizer on silicon-on-insulator platform," *Optics Express,* vol. 21, no. 10, pp. 12790-12796, 2013/05/20, 2013.
12. J. Guo, Y. Liu, L. Lin, S. Li, J. Cai, J. Chen, W. Huang, Y. Lin, and J. Xu, "Chromatic Plasmonic Polarizer-Based Synapse for All-Optical Convolutional Neural Network," *Nano Letters,* vol. 23, no. 20, pp. 9651-9656, 2023/10/25, 2023.
13. S. Wang, S. Wen, Z.-L. Deng, X. Li, and Y. Yang, "Metasurface-Based Solid Poincaré Sphere Polarizer," *Physical Review Letters,* vol. 130, no. 12, pp. 123801, 03/23/, 2023.
14. H. Lin, Y. Song, Y. Huang, D. Kita, S. Deckoff-Jones, K. Wang, L. Li, J. Li, H. Zheng, Z. Luo, H. Wang, S. Novak, A. Yadav, C.-C. Huang, R.-J. Shiue, D. Englund, T. Gu, D. Hewak, K. Richardson, J. Kong, and J. Hu, "Chalcogenide glass-on-graphene photonics," *Nature Photonics,* vol. 11, no. 12, pp. 798-805, 2017/12/01, 2017.
15. J. T. Kim, and H. Choi, "Polarization Control in Graphene-Based Polymer Waveguide Polarizer," *Laser & Photonics Reviews,* vol. 12, no. 10, pp. 1800142, 2018.
16. J. T. Kim, and C.-G. Choi, "Graphene-based polymer waveguide polarizer," *Optics Express,* vol. 20, no. 4, pp. 3556-3562, 2012/02/13, 2012.
17. J. Wu, Y. Yang, Y. Qu, X. Xu, Y. Liang, S. T. Chu, B. E. Little, R. Morandotti, B. Jia, and D. J. Moss, "Graphene Oxide Waveguide and Micro-Ring Resonator Polarizers," *Laser & Photonics Reviews,* vol. 13, no. 9, pp. 1900056, 2019.

 doi:10.20944/preprints202505.2452.v1




18. D. Jin, J. Wu, J. Hu, W. Liu, Y. Zhang, Y. Yang, L. Jia, D. Huang, B. Jia, and D. J. Moss, "Silicon photonic waveguide and microring resonator polarizers incorporating 2D graphene oxide films," *Applied Physics Letters,* vol. 125, no. 5, 2024.
19. W. H. Lim, Y. K. Yap, W. Y. Chong, C. H. Pua, N. M. Huang, R. M. De La Rue, and H. Ahmad, "Graphene oxide-based waveguide polariser: From thin film to quasi-bulk," *Optics Express,* vol. 22, no. 9, pp. 11090-11098, 2014/05/05, 2014.
20. L. Zhuo, D. Li, W. Chen, Y. Zhang, W. Zhang, Z. Lin, H. Zheng, W. Zhu, Y. Zhong, J. Tang, G. Lu, W. Fang, J. Yu, and Z. Chen, "High performance multifunction-in-one optoelectronic device by integrating graphene/MoS2 heterostructures on side-polished fiber," *Nanophotonics,* vol. 11, no. 6, pp. 1137-1147, 2022.
21. Y. Tan, R. He, C. Cheng, D. Wang, Y. Chen, and F. Chen, "Polarization-dependent optical absorption of MoS2 for refractive index sensing," *Scientific Reports,* vol. 4, no. 1, pp. 7523, 2014/12/17, 2014.
22. S. Sathiyan, H. Ahmad, W. Y. Chong, S. H. Lee, and S. Sivabalan, "Evolution of the Polarizing Effect of MoS2," *IEEE Photonics Journal,* vol. 7, no. 6, pp. 1-10, 2015.
23. Q. H. Wang, K. Kalantar-Zadeh, A. Kis, J. N. Coleman, and M. S. Strano, "Electronics and optoelectronics of two-dimensional transition metal dichalcogenides," *Nature Nanotechnology,* vol. 7, no. 11, pp. 699-712, 2012/11/01, 2012.
24. F. Xia, H. Wang, D. Xiao, M. Dubey, and A. Ramasubramaniam, "Two-dimensional material nanophotonics," *Nature Photonics,* vol. 8, no. 12, pp. 899-907, 2014/12/01, 2014.
25. S.-S. Chee, D. Seo, H. Kim, H. Jang, S. Lee, S. P. Moon, K. H. Lee, S. W. Kim, H. Choi, and M.-H. Ham, "Lowering the Schottky Barrier Height by Graphene/Ag Electrodes for High-Mobility MoS2 Field-Effect Transistors," *Advanced Materials,* vol. 31, no. 2, pp. 1804422, 2019.
26. B. Radisavljevic, A. Radenovic, J. Brivio, V. Giacometti, and A. Kis, "Single-layer MoS2 transistors," *Nature Nanotechnology,* vol. 6, no. 3, pp. 147-150, 2011/03/01, 2011.
27. J. Jiang, C. Ling, T. Xu, W. Wang, X. Niu, A. Zafar, Z. Yan, X. Wang, Y. You, L. Sun, J. Lu, J. Wang, and Z. Ni, "Defect Engineering for Modulating the Trap States in 2D Photoconductors," *Advanced Materials,* vol. 30, no. 40, pp. 1804332, 2018.
28. O. Lopez-Sanchez, D. Lembke, M. Kayci, A. Radenovic, and A. Kis, "Ultrasensitive photodetectors based on monolayer MoS2," *Nature Nanotechnology,* vol. 8, no. 7, pp. 497-501, 2013/07/01, 2013.
29. A. Hasani, M. Tekalgne, Q. V. Le, H. W. Jang, and S. Y. Kim, "Two-dimensional materials as catalysts for solar fuels: hydrogen evolution reaction and CO2 reduction," *Journal of Materials Chemistry A,* vol. 7, no. 2, pp. 430-454, 2019.
30. M. Asadi, K. Kim, C. Liu, A. V. Addepalli, P. Abbasi, P. Yasaei, P. Phillips, A. Behranginia, J. M. Cerrato, R. Haasch, P. Zapol, B. Kumar, R. F. Klie, J. Abiade, L. A. Curtiss, and A. Salehi-Khojin, "Nanostructured transition metal dichalcogenide electrocatalysts for CO<sub>2</sub> reduction in ionic liquid," *Science,* vol. 353, no. 6298, pp. 467-470, 2016.
31. S. Presolski, and M. Pumera, "Covalent functionalization of MoS2," *Materials Today,* vol. 19, no. 3, pp. 140-145, 2016/04/01/, 2016.
32. D.-M. Tang, D. G. Kvashnin, S. Najmaei, Y. Bando, K. Kimoto, P. Koskinen, P. M. Ajayan, B. I. Yakobson, P. B. Sorokin, J. Lou, and D. Golberg, "Nanomechanical cleavage of molybdenum disulphide atomic layers," *Nature Communications,* vol. 5, no. 1, pp. 3631, 2014/04/03, 2014.
33. K. F. Mak, C. Lee, J. Hone, J. Shan, and T. F. Heinz, "Atomically Thin MoS2: A New Direct-Gap Semiconductor," *Physical Review Letters,* vol. 105, no. 13, pp. 136805, 09/24/, 2010.
34. I. H. Abidi, S. P. Giridhar, J. O. Tollerud, J. Limb, M. Waqar, A. Mazumder, E. L. Mayes, B. J. Murdoch, C. Xu, A. Bhoriya, A. Ranjan, T. Ahmed, Y. Li, J. A. Davis, C. L. Bentley, S. P. Russo, E. D. Gaspera, and S. Walia, "Oxygen Driven Defect Engineering of Monolayer MoS2 for Tunable Electronic, Optoelectronic, and Electrochemical Devices," *Advanced Functional Materials,* vol. 34, no. 37, pp. 2402402, 2024.
35. I. H. Abidi, A. Bhoriya, P. Vashishtha, S. P. Giridhar, E. L. H. Mayes, M. Sehrawat, A. K. Verma, V. Aggarwal, T. Gupta, H. K. Singh, T. Ahmed, N. Dilawar Sharma, and S. Walia, "Oxidation-induced modulation of photoresponsivity in monolayer MoS2 with sulfur vacancies," *Nanoscale,* vol. 16, no. 42, pp. 19834-19843, 2024.

 doi:10.20944/preprints202505.2452.v1




36. K. M. Islam, R. Synowicki, T. Ismael, I. Oguntoye, N. Grinalds, and M. D. Escarra, "In-Plane and Out-of-Plane Optical Properties of Monolayer, Few-Layer, and Thin-Film MoS2 from 190 to 1700 nm and Their Application in Photonic Device Design," *Advanced Photonics Research,* vol. 2, no. 5, pp. 2000180, 2021.
37. G. A. Ermolaev, D. V. Grudinin, Y. V. Stebunov, K. V. Voronin, V. G. Kravets, J. Duan, A. B. Mazitov, G. I. Tselikov, A. Bylinkin, D. I. Yakubovsky, S. M. Novikov, D. G. Baranov, A. Y. Nikitin, I. A. Kruglov, T. Shegai, P. Alonso-González, A. N. Grigorenko, A. V. Arsenin, K. S. Novoselov, and V. S. Volkov, "Giant optical anisotropy in transition metal dichalcogenides for next-generation photonics," *Nature Communications,* vol. 12, no. 1, pp. 854, 2021/02/08, 2021.
38. Q. Feng, H. Cong, B. Zhang, W. Wei, Y. Liang, S. Fang, T. Wang, and J. Zhang, "Enhanced optical Kerr nonlinearity of graphene/Si hybrid waveguide," *Applied Physics Letters,* vol. 114, no. 7, 2019.
39. H. Cai, Y. Cheng, H. Zhang, Q. Huang, J. Xia, R. Barille, and Y. Wang, "Enhanced linear absorption coefficient of in-plane monolayer graphene on a silicon microring resonator," *Optics Express,* vol. 24, no. 21, pp. 24105-24116, 2016/10/17, 2016.
40. C. Martella, C. Mennucci, E. Cinquanta, A. Lamperti, E. Cappelluti, F. Buatier de Mongeot, and A. Molle, "Anisotropic MoS2 Nanosheets Grown on Self-Organized Nanopatterned Substrates," *Advanced Materials,* vol. 29, no. 19, pp. 1605785, 2017.
41. G.-H. Nam, Q. He, X. Wang, Y. Yu, J. Chen, K. Zhang, Z. Yang, D. Hu, Z. Lai, B. Li, Q. Xiong, Q. Zhang, L. Gu, and H. Zhang, "In-Plane Anisotropic Properties of 1T′ -MoS2 Layers," *Advanced Materials,* vol. 31, no. 21, pp. 1807764, 2019.
42. Y. Zhang, J. Wu, L. Jia, D. Jin, B. Jia, X. Hu, D. Moss, and Q. Gong, "Advanced optical polarizers based on 2D materials," *npj Nanophotonics,* vol. 1, no. 1, pp. 28, 2024/07/17, 2024.
43. L. Jia, J. Wu, Y. Zhang, Y. Qu, B. Jia, Z. Chen, and D. J. Moss, "Fabrication Technologies for the On-Chip Integration of 2D Materials," *Small Methods,* vol. 6, no. 3, pp. 2101435, 2022.
44. A. Gurarslan, Y. Yu, L. Su, Y. Yu, F. Suarez, S. Yao, Y. Zhu, M. Ozturk, Y. Zhang, and L. Cao, "Surface-Energy-Assisted Perfect Transfer of Centimeter-Scale Monolayer and Few-Layer MoS2 Films onto Arbitrary Substrates," *ACS Nano,* vol. 8, no. 11, pp. 11522-11528, 2014/11/25, 2014.
45. W. M. Parkin, A. Balan, L. Liang, P. M. Das, M. Lamparski, C. H. Naylor, J. A. Rodríguez-Manzo, A. T. C. Johnson, V. Meunier, and M. Drndić, "Raman Shifts in Electron-Irradiated Monolayer MoS2," *ACS Nano,* vol. 10, no. 4, pp. 4134-4142, 2016/04/26, 2016.
46. J. Zhang, H. Yu, W. Chen, X. Tian, D. Liu, M. Cheng, G. Xie, W. Yang, R. Yang, X. Bai, D. Shi, and G. Zhang, "Scalable Growth of High-Quality Polycrystalline MoS2 Monolayers on SiO2 with Tunable Grain Sizes," *ACS Nano,* vol. 8, no. 6, pp. 6024-6030, 2014/06/24, 2014.
47. L. Britnell, R. M. Ribeiro, A. Eckmann, R. Jalil, B. D. Belle, A. Mishchenko, Y.-J. Kim, R. V. Gorbachev, T. Georgiou, S. V. Morozov, A. N. Grigorenko, A. K. Geim, C. Casiraghi, A. H. C. Neto, and K. S. Novoselov, "Strong Light-Matter Interactions in Heterostructures of Atomically Thin Films," *Science,* vol. 340, no. 6138, pp. 1311-1314, 2013.
48. D. Dumcenco, D. Ovchinnikov, K. Marinov, P. Lazić, M. Gibertini, N. Marzari, O. L. Sanchez, Y.-C. Kung, D. Krasnozhon, M.-W. Chen, S. Bertolazzi, P. Gillet, A. Fontcuberta i Morral, A. Radenovic, and A. Kis, "Large-Area Epitaxial Monolayer MoS2," *ACS Nano,* vol. 9, no. 4, pp. 4611-4620, 2015/04/28, 2015.
49. V. Forsberg, R. Zhang, J. Bäckström, C. Dahlström, B. Andres, M. Norgren, M. Andersson, M. Hummelgård, and H. Olin, "Exfoliated MoS2 in Water without Additives," *PLOS ONE,* vol. 11, no. 4, pp. e0154522, 2016.
50. X. Liu, T. Wang, G. Hu, C. Xu, Y. Xiong, and Y. Wang, "Controllable synthesis of self-assembled MoS2 hollow spheres for photocatalytic application," *Journal of Materials Science: Materials in Electronics,* vol. 29, no. 1, pp. 753-761, 2018/01/01, 2018.
51. H. Liu, D. Su, R. Zhou, B. Sun, G. Wang, and S. Z. Qiao, "Highly Ordered Mesoporous MoS2 with Expanded Spacing of the (002) Crystal Plane for Ultrafast Lithium Ion Storage," *Advanced Energy Materials,* vol. 2, no. 8, pp. 970-975, 2012.
52. C. P. Veeramalai, F. Li, Y. Liu, Z. Xu, T. Guo, and T. W. Kim, "Enhanced field emission properties of molybdenum disulphide few layer nanosheets synthesized by hydrothermal method," *Applied Surface Science,* vol. 389, pp. 1017-1022, 2016/12/15/, 2016.

 doi:10.20944/preprints202505.2452.v1




53. H. Nan, Z. Wang, W. Wang, Z. Liang, Y. Lu, Q. Chen, D. He, P. Tan, F. Miao, X. Wang, J. Wang, and Z. Ni, "Strong Photoluminescence Enhancement of MoS2 through Defect Engineering and Oxygen Bonding," *ACS Nano*, vol. 8, no. 6, pp. 5738-5745, 2014/06/24, 2014.
54. S.-S. Chee, W.-J. Lee, Y.-R. Jo, M. K. Cho, D. Chun, H. Baik, B.-J. Kim, M.-H. Yoon, K. Lee, and M.-H. Ham, "Atomic Vacancy Control and Elemental Substitution in a Monolayer Molybdenum Disulfide for High Performance Optoelectronic Device Arrays," *Advanced Functional Materials*, vol. 30, no. 11, pp. 1908147, 2020.
55. N. Jiménez-Arévalo, J. H. Al Shuhaib, R. B. Pacheco, D. Marchiani, M. M. Saad Abdelnabi, R. Frisenda, M. Sbroscia, M. G. Betti, C. Mariani, Y. Manzanares-Negro, C. G. Navarro, A. J. Martínez-Galera, J. R. Ares, I. J. Ferrer, and F. Leardini, "MoS2 Photoelectrodes for Hydrogen Production: Tuning the S-Vacancy Content in Highly Homogeneous Ultrathin Nanocrystals," *ACS Applied Materials & Interfaces*, vol. 15, no. 28, pp. 33514-33524, 2023/07/19, 2023.
56. D. Dai, J. Bauters, and J. E. Bowers, "Passive technologies for future large-scale photonic integrated circuits on silicon: polarization handling, light non-reciprocity and loss reduction," *Light: Science & Applications*, vol. 1, no. 3, pp. e1-e1, 2012/03/01, 2012.
57. J. Wu, Y. Zhang, J. Hu, Y. Yang, D. Jin, W. Liu, D. Huang, B. Jia, and D. J. Moss, "2D graphene oxide films expand functionality of photonic chips," *Advanced Materials*, pp. 2403659, 2024.
58. Y. Zhang, L. Tao, D. Yi, J.-b. Xu, and H. K. Tsang, "Enhanced thermo-optic nonlinearities in a MoS2-on-silicon microring resonator," *Applied Physics Express*, vol. 13, no. 2, pp. 022004, 2020/01/08, 2020.
59. H. Li, Y. Anugrah, S. J. Koester, and M. Li, "Optical absorption in graphene integrated on silicon waveguides," *Applied Physics Letters*, vol. 101, no. 11, 2012.
60. Y. Zhang, J. Wu, Y. Yang, Y. Qu, L. Jia, T. Moein, B. Jia, and D. J. Moss, "Enhanced Kerr Nonlinearity and Nonlinear Figure of Merit in Silicon Nanowires Integrated with 2D Graphene Oxide Films," *ACS Applied Materials & Interfaces*, vol. 12, no. 29, pp. 33094-33103, 2020/07/22, 2020.
61. C. Pei, L. Yang, G. Wang, Y. Wang, X. Jiang, Y. Hao, Y. Li, and J. Yang, "Broadband Graphene/Glass Hybrid Waveguide Polarizer," *IEEE Photonics Technology Letters*, vol. 27, no. 9, pp. 927-930, 2015.
62. J. Hu, J. Wu, D. Jin, W. Liu, Y. Zhang, Y. Yang, L. Jia, Y. Wang, D. Huang, B. Jia, and D. J. Moss, "Integrated photonic polarizers with 2D reduced graphene oxide," *Opto-Electronic Science*, pp. 240032, 2025/02/26, 2025.
63. A. Rickman, "The commercialization of silicon photonics," *Nature Photonics*, vol. 8, no. 8, pp. 579-582, 2014/08/01, 2014.
64. J. Leuthold, C. Koos, and W. Freude, "Nonlinear silicon photonics," *Nature Photonics*, vol. 4, no. 8, pp. 535-544, 2010/08/01, 2010.
65. D. J. Moss, R. Morandotti, A. L. Gaeta, and M. Lipson, "New CMOS-compatible platforms based on silicon nitride and Hydex for nonlinear optics," *Nature Photonics*, vol. 7, no. 8, pp. 597-607, 2013/08/01, 2013.
66. L. Razzari, et al., "CMOS-compatible integrated optical hyper-parametric oscillator," Nature Photonics, vol. 4, no. 1, pp. 41-45, 2010.
67. A. Pasquazi, et al., "Sub-picosecond phase-sensitive optical pulse characterization on a chip", Nature Photonics, vol. 5, no. 10, pp. 618-623 (2011).
68. M Ferrera et al., "On-Chip ultra-fast 1st and 2nd order CMOS compatible all-optical integration", Optics Express vol. 19 (23), 23153-23161 (2011).
69. Bao, C., et al., Direct soliton generation in microresonators, Opt. Lett, 42, 2519 (2017).
70. M.Ferrera et al., "CMOS compatible integrated all-optical RF spectrum analyzer", Optics Express, vol. 22, no. 18, 21488 - 21498 (2014).
71. M. Kues, et al., "Passively modelocked laser with an ultra-narrow spectral width", Nature Photonics, vol. 11, no. 3, pp. 159, 2017.
72. M. Ferrera, et al., "Low-power continuous-wave nonlinear optics in doped silica glass integrated waveguide structures," Nature Photonics, vol. 2, no. 12, pp. 737-740, 2008.
73. M.Ferrera et al."On-Chip ultra-fast 1st and 2nd order CMOS compatible all-optical integration", Opt. Express, vol. 19, (23)pp. 23153-23161 (2011).
74. D. Duchesne, M. Peccianti, M. R. E. Lamont, et al., "Supercontinuum generation in a high index doped silica glass spiral waveguide," Optics Express, vol. 18, no, 2, pp. 923-930, 2010.

 doi:10.20944/preprints202505.2452.v1




75. H Bao, L Olivieri, M Rowley, ST Chu, BE Little, R Morandotti, DJ Moss, ... "Turing patterns in a fiber laser with a nested microresonator: Robust and controllable microcomb generation", Physical Review Research vol. 2 (2), 023395 (2020).
76. M. Ferrera, et al., "On-chip CMOS-compatible all-optical integrator", Nature Communications, vol. 1, Article 29, 2010.
77. A. Pasquazi, et al., "All-optical wavelength conversion in an integrated ring resonator," Optics Express, vol. 18, no. 4, pp. 3858-3863, 2010.
78. A.Pasquazi, Y. Park, J. Azana, et al., "Efficient wavelength conversion and net parametric gain via Four Wave Mixing in a high index doped silica waveguide," Optics Express, vol. 18, no. 8, pp. 7634-7641, 2010.
79. Peccianti, M. Ferrera, L. Razzari, et al., "Subpicosecond optical pulse compression via an integrated nonlinear chirper," Optics Express, vol. 18, no. 8, pp. 7625-7633, 2010.
80. M Ferrera, Y Park, L Razzari, BE Little, ST Chu, R Morandotti, DJ Moss, ... et al., "All-optical 1st and 2nd order integration on a chip", Optics Express vol. 19 (23), 23153-23161 (2011).
81. M. Ferrera et al., "Low Power CW Parametric Mixing in a Low Dispersion High Index Doped Silica Glass Micro-Ring Resonator with Q-factor > 1 Million", Optics Express, vol.17, no. 16, pp. 14098–14103 (2009).
82. M. Peccianti, et al., "Demonstration of an ultrafast nonlinear microcavity modelocked laser", Nature Communications, vol. 3, pp. 765, 2012.
83. A.Pasquazi, et al., "Self-locked optical parametric oscillation in a CMOS compatible microring resonator: a route to robust optical frequency comb generation on a chip," Optics Express, vol. 21, no. 11, pp. 13333-13341, 2013.
84. A.Pasquazi, et al., "Stable, dual mode, high repetition rate mode-locked laser based on a microring resonator," Optics Express, vol. 20, no. 24, pp. 27355-27362, 2012.
85. Pasquazi, A. et al. Micro-combs: a novel generation of optical sources. Physics Reports 729, 1-81 (2018).
86. H. Bao, et al., Laser cavity-soliton microcombs, Nature Photonics, vol. 13, no. 6, pp. 384-389, Jun. 2019.
87. Antonio Cutrona, Maxwell Rowley, Debayan Das, Luana Olivieri, Luke Peters, Sai T. Chu, Brent L. Little, Roberto Morandotti, David J. Moss, Juan Sebastian Totero Gongora, Marco Peccianti, Alessia Pasquazi, "High Conversion Efficiency in Laser Cavity-Soliton Microcombs", Optics Express Vol. 30, Issue 22, pp. 39816-39825 (2022). https://doi.org/10.1364/OE.470376.
88. A. Cutrona, M. Rowley, A. Bendahmane, V. Cecconi,L. Peters, L. Olivieri, B. E. Little, S. T. Chu, S. Stivala, R. Morandotti, D. J. Moss, J. S. Totero-Gongora, M. Peccianti, A. Pasquazi, "Nonlocal bonding of a soliton and a blue-detuned state in a microcomb laser", ***Nature Communications Physics*** **6** Article 259 (2023). https://doi.org/10.1038/s42005-023-01372-0.
89. Aadhi A. Rahim, Imtiaz Alamgir, Luigi Di Lauro, Bennet Fischer, Nicolas Perron, Pavel Dmitriev, Celine Mazoukh, Piotr Roztocki, Cristina Rimoldi, Mario Chemnitz, Armaghan Eshaghi, Evgeny A. Viktorov, Anton V. Kovalev, Brent E. Little, Sai T. Chu, David J. Moss, and Roberto Morandotti, "Mode-locked laser with multiple timescales in a microresonator-based nested cavity", ***APL Photonics*** **9** 031302 (2024). DOI:10.1063/5.0174697.
90. Andrew Cooper, Luana Olivieri, Antonio Cutrona, Debayan Das, Luke Peters, Sai Tak Chu, Brent Little, Roberto Morandotti, David J Moss, Marco Peccianti, and Alessia Pasquazi, "Parametric interaction of laser cavity-solitons with an external CW pump", ***Optics Express*** **32** (12), 21783-21794 (2024).
91. A. Cutrona, M. Rowley, A. Bendahmane, V. Cecconi,L. Peters, L. Olivieri, B. E. Little, S. T. Chu, S. Stivala, R. Morandotti, D. J. Moss, J. S. Totero-Gongora, M. Peccianti, A. Pasquazi, "Stability Properties of Laser Cavity-Solitons for Metrological Applications", Applied Physics Letters vol. 122 (12) 121104 (2023); doi: 10.1063/5.0134147.
92. Caitlin E. Murray, Mengxi Tan, Chawaphon Prayoonyong, Sai T. Chu, Brent E. Little, Roberto Morandotti, Arnan Mitchell, David J. Moss and Bill Corcoran, "Investigating the thermal robustness of soliton crystal microcombs", ***Optics Express*** **31**(23), 37749-37762 (2023).
93. Yonghang Sun, James Salamy, Caitlin E. Murry, Brent E. Little, Sai T. Chu, Roberto Morandotti, Arnan Mitchell, David J. Moss, Bill Corcoran, "Enhancing laser temperature stability by passive self-injection locking to a micro-ring resonator", ***Optics Express*** **32** (13) 23841-23855 (2024) https://doi.org/10.1364/OE.515269.

 doi:10.20944/preprints202505.2452.v1




94. Yonghang Sun, James Salamy, Caitlin E. Murray, Xiaotian Zhu, Brent E. Little, Roberto Morandotti, Arnan Mitchell, Sai T. Chu, David J. Moss, Bill Corcoran, "Self-locking of free-running DFB lasers to a single microring resonator for dense WDM", ***Journal of Lightwave Technology*** **43**, (4) 1995-2002 (2025). DOI: 10.1109/JLT.2024.3494694.
95. X. Xu, J. Wu, M. Shoeiby, T. G. Nguyen, S. T. Chu, B. E. Little, R. Morandotti, A. Mitchell, and D. J. Moss, "Reconfigurable broadband microwave photonic intensity differentiator based on an integrated optical frequency comb source," APL Photonics, vol. 2, no. 9, 096104, Sep. 2017.
96. Xu, X., et al., Photonic microwave true time delays for phased array antennas using a 49 GHz FSR integrated micro-comb source, Photonics Research, vol. 6, B30-B36 (2018).
97. X. Xu, M. Tan, J. Wu, R. Morandotti, A. Mitchell, and D. J. Moss, "Microcomb-based photonic RF signal processing", IEEE Photonics Technology Letters, vol. 31 no. 23 1854-1857, 2019.
98. Xu, et al., "Advanced adaptive photonic RF filters with 80 taps based on an integrated optical micro-comb source," Journal of Lightwave Technology, vol. 37, no. 4, pp. 1288-1295 (2019).
99. X. Xu, et al., "Photonic RF and microwave integrator with soliton crystal microcombs", IEEE Transactions on Circuits and Systems II: Express Briefs, vol. 67, no. 12, pp. 3582-3586, 2020. DOI:10.1109/TCSII.2020.2995682.
100. X. Xu, et al., "High performance RF filters via bandwidth scaling with Kerr micro-combs," APL Photonics, vol. 4 (2) 026102. 2019.
101. M. Tan, et al., "Microwave and RF photonic fractional Hilbert transformer based on a 50 GHz Kerr micro-comb", Journal of Lightwave Technology, vol. 37, no. 24, pp. 6097 – 6104, 2019.
102. M. Tan, et al., "RF and microwave fractional differentiator based on photonics", IEEE Transactions on Circuits and Systems: Express Briefs, vol. 67, no.11, pp. 2767-2771, 2020. DOI:10.1109/TCSII.2020.2965158.
103. M. Tan, et al., "Photonic RF arbitrary waveform generator based on a soliton crystal micro-comb source", Journal of Lightwave Technology, vol. 38, no. 22, pp. 6221-6226 (2020). DOI: 10.1109/JLT.2020.3009655.
104. M. Tan, X. Xu, J. Wu, R. Morandotti, A. Mitchell, and D. J. Moss, "RF and microwave high bandwidth signal processing based on Kerr Micro-combs", Advances in Physics X, VOL. 6, NO. 1, 1838946 (2021). DOI:10.1080/23746149.2020.1838946.
105. X. Xu, et al., "Advanced RF and microwave functions based on an integrated optical frequency comb source," Opt. Express, vol. 26 (3) 2569 (2018).
106. M. Tan, X. Xu, J. Wu, B. Corcoran, A. Boes, T. G. Nguyen, S. T. Chu, B. E. Little, R. Morandotti, A. Lowery, A. Mitchell, and D. J. Moss, ""Highly Versatile Broadband RF Photonic Fractional Hilbert Transformer Based on a Kerr Soliton Crystal Microcomb", Journal of Lightwave Technology vol. 39 (24) 7581-7587 (2021).
107. Wu, J. et al. RF Photonics: An Optical Microcombs' Perspective. IEEE Journal of Selected Topics in Quantum Electronics Vol. 24, 6101020, 1-20 (2018).
108. T. G. Nguyen et al., "Integrated frequency comb source-based Hilbert transformer for wideband microwave photonic phase analysis," Opt. Express, vol. 23, no. 17, pp. 22087-22097, Aug. 2015.
109. X. Xu, et al., "Broadband RF channelizer based on an integrated optical frequency Kerr comb source," Journal of Lightwave Technology, vol. 36, no. 19, pp. 4519-4526, 2018.
110. X. Xu, et al., "Continuously tunable orthogonally polarized RF optical single sideband generator based on micro-ring resonators," Journal of Optics, vol. 20, no. 11, 115701. 2018.
111. X. Xu, et al., "Orthogonally polarized RF optical single sideband generation and dual-channel equalization based on an integrated microring resonator," Journal of Lightwave Technology, vol. 36, no. 20, pp. 4808-4818. 2018.
112. X. Xu, et al., "Photonic RF phase-encoded signal generation with a microcomb source", J. Lightwave Technology, vol. 38, no. 7, 1722-1727, 2020.
113. X. Xu, et al., Broadband microwave frequency conversion based on an integrated optical micro-comb source", Journal of Lightwave Technology, vol. 38 no. 2, pp. 332-338, 2020.
114. M. Tan, et al., "Photonic RF and microwave filters based on 49GHz and 200GHz Kerr microcombs", Optics Comm. vol. 465,125563, Feb. 22. 2020.

 doi:10.20944/preprints202505.2452.v1




115. X. Xu, et al., "Broadband photonic RF channelizer with 90 channels based on a soliton crystal microcomb", Journal of Lightwave Technology, Vol. 38, no. 18, pp. 5116 – 5121 (2020). doi: 10.1109/JLT.2020.2997699.
116. M. Tan et al, "Orthogonally polarized Photonic Radio Frequency single sideband generation with integrated micro-ring resonators", IOP Journal of Semiconductors, Vol. 42 (4), 041305 (2021). DOI: 10.1088/1674-4926/42/4/041305.
117. Mengxi Tan, X. Xu, J. Wu, T. G. Nguyen, S. T. Chu, B. E. Little, R. Morandotti, A. Mitchell, and David J. Moss, "Photonic Radio Frequency Channelizers based on Kerr Optical Micro-combs", IOP Journal of Semiconductors Vol. 42 (4), 041302 (2021). DOI:10.1088/1674-4926/42/4/041302.
118. B. Corcoran, et al., "Ultra-dense optical data transmission over standard fiber with a single chip source", Nature Communications, vol. 11, Article:2568, 2020.
119. X. Xu et al, "Photonic perceptron based on a Kerr microcomb for scalable high speed optical neural networks", Laser and Photonics Reviews, vol. 14, no. 8, 2000070 (2020). DOI: 10.1002/lpor.202000070.
120. X. Xu, et al., "11 TOPs photonic convolutional accelerator for optical neural networks", Nature vol. 589, 44-51 (2021).
121. Xingyuan Xu, Weiwei Han, Mengxi Tan, Yang Sun, Yang Li, Jiayang Wu, Roberto Morandotti, Arnan Mitchell, Kun Xu, and David J. Moss, "Neuromorphic computing based on wavelength-division multiplexing", ***IEEE Journal of Selected Topics in Quantum Electronics*** **29** (2) 7400112 (2023). DOI:10.1109/JSTQE.2022.3203159.
122. Yunping Bai, Xingyuan Xu,1, Mengxi Tan, Yang Sun, Yang Li, Jiayang Wu, Roberto Morandotti, Arnan Mitchell, Kun Xu, and David J. Moss, "Photonic multiplexing techniques for neuromorphic computing", Nanophotonics vol. 12 (5): 795–817 (2023). DOI:10.1515/nanoph-2022-0485.
123. Chawaphon Prayoonyong, Andreas Boes, Xingyuan Xu, Mengxi Tan, Sai T. Chu, Brent E. Little, Roberto Morandotti, Arnan Mitchell, David J. Moss, and Bill Corcoran, "Frequency comb distillation for optical superchannel transmission", Journal of Lightwave Technology vol. 39 (23) 7383-7392 (2021). DOI: 10.1109/JLT.2021.3116614.
124. Mengxi Tan, Xingyuan Xu, Jiayang Wu, Bill Corcoran, Andreas Boes, Thach G. Nguyen, Sai T. Chu, Brent E. Little, Roberto Morandotti, Arnan Mitchell, and David J. Moss, "Integral order photonic RF signal processors based on a soliton crystal micro-comb source", IOP Journal of Optics vol. 23 (11) 125701 (2021). https://doi.org/10.1088/2040-8986/ac2eab
125. Yang Sun, Jiayang Wu, Yang Li, Xingyuan Xu, Guanghui Ren, Mengxi Tan, Sai Tak Chu, Brent E. Little, Roberto Morandotti, Arnan Mitchell, and David J. Moss, "Optimizing the performance of microcomb based microwave photonic transversal signal processors", Journal of Lightwave Technology vol. 41 (23) pp 7223-7237 (2023). DOI: 10.1109/JLT.2023.3314526.
126. Mengxi Tan, Xingyuan Xu, Andreas Boes, Bill Corcoran, Thach G. Nguyen, Sai T. Chu, Brent E. Little, Roberto Morandotti, Jiayang Wu, Arnan Mitchell, and David J. Moss, "Photonic signal processor for real-time video image processing based on a Kerr microcomb", ***Nature Communications Engineering*** **2** 94 (2023). DOI:10.1038/s44172-023-00135-7.
127. Mengxi Tan, Xingyuan Xu, Jiayang Wu, Roberto Morandotti, Arnan Mitchell, and David J. Moss, "Photonic RF and microwave filters based on 49GHz and 200GHz Kerr microcombs", Optics Communications, vol. 465, Article: 125563 (2020). doi:10.1016/j.optcom.2020.125563. doi.org/10.1063/1.5136270.
128. Yang Sun, Jiayang Wu, Yang Li, Mengxi Tan, Xingyuan Xu, Sai Chu, Brent Little, Roberto Morandotti, Arnan Mitchell, and David J. Moss, "Quantifying the Accuracy of Microcomb-based Photonic RF Transversal Signal Processors", IEEE Journal of Selected Topics in Quantum Electronics vol. 29 no. 6, pp. 1-17, Art no. 7500317 (2023). 10.1109/JSTQE.2023.3266276.
129. Yang Li, Yang Sun, Jiayang Wu, Guanghui Ren, Bill Corcoran, Xingyuan Xu, Sai T. Chu, Brent. E. Little, Roberto Morandotti, Arnan Mitchell, and David J. Moss, "Processing accuracy of microcomb-based microwave photonic signal processors for different input signal waveforms", ***MDPI Photonics*** ***10***, 10111283 (2023). DOI:10.3390/photonics10111283
130. Yang Sun, Jiayang Wu, Yang Li, and David J. Moss, "Comparison of microcomb-based RF photonic transversal signal processors implemented with discrete components versus integrated chips", ***MDPI Micromachines*** **14**, 1794 (2023). https://doi.org/10.3390/mi14091794

 doi:10.20944/preprints202505.2452.v1




131. Mengxi Tan, David J. Moss, "The laser trick that could put an ultraprecise optical clock on a chip", ***Nature*** **624**, (7991) 256-257 (2023). *doi.org/10.1038/d41586-023-03782-0.*
132. Weiwei Han, Zhihui Liu, Yifu Xu, Mengxi Tan, Chaoran Huang, Jiayang Wu, Kun Xu, David J. Moss, and Xingyuan Xu, "Photonic RF Channelization Based on Microcombs", ***IEEE Journal of Selected Topics in Quantum Electronics*** **30** (5) 7600417 (2024). DOI:10.1109/JSTQE.2024.3398419.
133. Yang Li, Yang Sun, Jiayang Wu, Guanghui Ren, Xingyuan Xu, Mengxi Tan, Sai Chu, Brent Little, Roberto Morandotti, Arnan Mitchell, and David Moss, "Feedback control in micro-comb-based microwave photonic transversal filter systems", ***IEEE Journal of Selected Topics in Quantum Electronics*** Vol. **30** (5) 2900117 (2024). DOI: 10.1109/JSTQE.2024.3377249.
134. Weiwei Han, Zhihui Liu, Yifu Xu, Mengxi Tan, Yuhua Li, Xiaotian Zhu, Yanni Ou, Feifei Yin, Roberto Morandotti, Brent E. Little, Sai Tak Chu, Xingyuan Xu, David J. Moss, and Kun Xu, "Dual-polarization RF Channelizer Based on Microcombs", ***Optics Express*** **32**, No. 7, 11281-11295 (2024). DOI: 10.1364/OE.519235.
135. Zhihui Liu, Haoran Zhang, Yuhang Song, Xiaotian Zhu, Yunping Bai, Mengxi Tan, Bill Corcoran, Caitlin Murphy, Sai T. Chu, David J. Moss, Xingyuan Xu, and Kun Xu, "Advances in Soliton Crystals Microcombs", Photonics Vol. 11, 1164 (2024). https://doi.org/10.3390/photonics11121164.
136. C. Mazoukh, L. Di Lauro, I. Alamgir1 B. Fischer, A. Aadhi, A. Eshaghi, B. E. Little, S. T. Chu, D. J. Moss, and R. Morandotti, "Genetic algorithm-enhanced microcomb state generation", ***Nature Communications Physics*** Vol. 7, Article: 81 (2024). DOI: 10.1038/s42005-024-01558-0.
137. Shifan Chen, Yixuan Zheng, Yifu Xu, Xiaotian Zhu, Sirui Huang, Shuai Wang, Xiaoyan Xu, Chengzhuo Xia, Zhihui Liu, Chaoran Huang, Roberto Morandotti, Sai T. Chu, Brent E. Little, Bill Corcoran, Yuyang Liu, Yunping Bai, David J. Moss, Xingyuan Xu, and Kun Xu, "High-bit-efficiency TOPS optical tensor convolutional accelerator using micro-combs", ***Laser & Photonics Reviews*** **19** 2401975 (2025). DOI: 10.1002/lpor.202401975
138. Weiwei Han, Zhihui Liu, Yifu Xu, Mengxi Tan, Yuhua Li, Xiaotian Zhu, Yanni Ou, Feifei Yin, Roberto Morandotti, Brent E. Little, Sai Tak Chu, David J. Moss, Xingyuan Xu, and Kun Xu, "TOPS-speed complex-valued convolutional accelerator for feature extraction and inference", ***Nature Communications*** **16** 292 (2025). DOI: 10.1038/s41467-024-55321-8.
139. Yang Li, Yang Sun, Jiayang Wu, Guanghui Ren, Roberto Morandotti, Xingyuan Xu, Mengxi Tan, Arnan Mitchell, and David J. Moss, "Performance analysis of microwave photonic spectral filters based on optical microcombs", ***Advanced Physics Research*** **4** (9) 2400084 (2025). DOI:10.1002/apxr.202400084.
140. Luigi di Lauro, Stefania Sciara, Bennet Fischer, Junliang Dong, Imtiaz Alamgir, Benjamin Wetzel, Goëry Genty, Mitchell Nichols, Armaghan Eshaghi, David J. Moss, Roberto Morandotti, "Optimization Methods for Integrated and Programmable Photonics in Next-Generation Classical and Quantum Smart Communication and Signal Processing", ***Advances in Optics and Photonics*** Vol. **17** (2) (2025).
141. Bill Corcoran, Arnan Mitchell, Roberto Morandotti, Leif K. Oxenlowe, and David J. Moss, "Optical microcombs for ultrahigh-bandwidth communications", ***Nature Photonics*** Volume **19** (5) 451 - 462 (2025). DOI: 10.1038/s41566-025-01662-9.
142. Qihang Ai, Mengxi Tan, Hanxiao Feng, Xinyu Yang, Xingyuan Xu, Roberto Morandotti, Arnan Mitchell, Donglin Su, and David J. Moss, "Photonic real-time signal processing", ***Nanophotonics*** **29** (2025).
143. Xingyuan Xu, Jiajia Wang, Xiaotian Zhu, Yifu Xu, Shifan Chen, Haoran Zhang, Shuying Li, Yunping Bai, Zhihui Liu, Roberto Morandotti, Brent E. Little, Arthur J. Lowery, David J. Moss, Sai T. Chu, and Kun Xu, "Microcomb-enabled parallel self- calibration optical convolution streaming processor", ***Light Science and Applications*** (2025).
144. Shifan Chen, Yixuan Zheng, Yifu Xu, Xiaotian Zhu, Sirui Huang, Shuai Wang, Xiaoyan Xu, Chengzhuo Xia, Zhihui Liu, Chaoran Huang, Roberto Morandotti, Sai T. Chu, Brent E. Little, Bill Corcoran, Yuyang Liu, Yunping Bai, David J. Moss, Xingyuan Xu, and Kun Xu, "Integrated photonic neural networks", ***npj Nanophotonics*** **2**, 28 (2025).
145. M. Rowley, Pierre-Henry Hanzard, Antonio Cutrona, Hualong Bao, Sai T. Chu, Brent E. Little, Roberto Morandotti, David J. Moss, Gian-Luca Oppo, Juan Sebastian Totero Gongora, Marco Peccianti and Alessia Pasquazi, "Self-emergence of robust solitons in a micro-cavity", Nature **608** (7922) 303 – 309 (2022).

 doi:10.20944/preprints202505.2452.v1




146. Hamed Arianfard, Saulius Juodkazis, David J. Moss, and Jiayang Wu, "Sagnac interference in integrated photonics", ***Applied Physics Reviews*** **10** (1) 011309 (2023). doi: 10.1063/5.0123236.
147. Hamed Arianfard, Jiayang Wu, Saulius Juodkazis, and David J. Moss, "Optical analogs of Rabi splitting in integrated waveguide-coupled resonators", ***Advanced Physics Research*** **2** 2200123 (2023). DOI: 10.1002/apxr.202200123.
148. Hamed Arianfard, Jiayang Wu, Saulius Juodkazis, and David J. Moss, "Spectral shaping based on optical waveguides with advanced Sagnac loop reflectors", Paper No. PW22O-OE201-20, SPIE-Opto, Integrated Optics: Devices, Materials, and Technologies XXVI, SPIE Photonics West, San Francisco CA January 22 - 27 (2022). doi: 10.1117/12.2607902
149. Hamed Arianfard, Jiayang Wu, Saulius Juodkazis, David J. Moss, "Spectral Shaping Based on Integrated Coupled Sagnac Loop Reflectors Formed by a Self-Coupled Wire Waveguide", IEEE Photonics Technology Letters vol. 33 (13) 680-683 (2021). DOI:10.1109/LPT.2021.3088089.
150. Hamed Arianfard, Jiayang Wu, Saulius Juodkazis and David J. Moss, "Three Waveguide Coupled Sagnac Loop Reflectors for Advanced Spectral Engineering", Journal of Lightwave Technology vol. 39 (11) 3478-3487 (2021). DOI: 10.1109/JLT.2021.3066256.
151. Hamed Arianfard, Jiayang Wu, Saulius Juodkazis and David J. Moss, "Advanced Multi-Functional Integrated Photonic Filters based on Coupled Sagnac Loop Reflectors", Journal of Lightwave Technology vol. 39 Issue: 5, pp.1400-1408 (2021). DOI:10.1109/JLT.2020.3037559.
152. Hamed Arianfard, Jiayang Wu, Saulius Juodkazis and David J. Moss, "Advanced multi-functional integrated photonic filters based on coupled Sagnac loop reflectors", Paper 11691-4, PW21O-OE203-44, Silicon Photonics XVI, SPIE Photonics West, San Francisco CA March 6-11 (2021). doi.org/10.1117/12.2584020
153. Jiayang Wu, Tania Moein, Xingyuan Xu, and David J. Moss, "Advanced photonic filters via cascaded Sagnac loop reflector resonators in silicon-on-insulator integrated nanowires", Applied Physics Letters Photonics vol. 3 046102 (2018).
154. J. Wu, H. Lin, D. J. Moss, K. P. Loh, and B. Jia, "Graphene oxide for photonics, electronics and optoelectronics," *Nature Reviews Chemistry,* vol. 7, no. 3, pp. 162-183, 2023/03/01, 2023.
155. Y. Zhang, J. Wu, L. Jia, Y. Qu, Y. Yang, B. Jia, and D. J. Moss, "Graphene Oxide for Nonlinear Integrated Photonics," *Laser & Photonics Reviews,* vol. 17, no. 3, pp. 2200512, 2023/03/01, 2023.
156. J. Hu, J. Wu, W. Liu, D. Jin, H. E. Dirani, S. Kerdiles, C. Sciancalepore, P. Demongodin, C. Grillet, C. Monat, D. Huang, B. Jia, and D. J. Moss, "2D graphene oxide: a versatile thermo-optic material," *Advanced Functional Materials,* vol. 34, no. 46, pp. 2406799, 2024.
157. J. Wu, L. Jia, Y. Zhang, Y. Qu, B. Jia, and D. J. Moss, "Graphene Oxide for Integrated Photonics and Flat Optics," *Advanced Materials,* vol. 33, no. 3, pp. 2006415, 2021.
158. Y. Zhang, J. Wu, Y. Yang, Y. Qu, L. Jia, T. Moein, B. Jia, and D. J. Moss, "Enhanced Kerr Nonlinearity and Nonlinear Figure of Merit in Silicon Nanowires Integrated with 2D Graphene Oxide Films," *ACS Applied Materials & Interfaces,* vol. 12, no. 29, pp. 33094-33103, 2020/07/22, 2020.
159. Junkai Hu, Jiayang Wu, Di Jin, Wenbo Liu, Yuning Zhang, Yunyi Yang, Linnan Jia, Duan Huang, Baohua Jia, and David J. Moss, "Integrated waveguide and microring polarizers incorporating 2D reduced graphene oxide", ***Opto-Electronic Science*** **4** 240032 (2025). DOI: 10.29026/oes.2025.240032
160. D. Jin, J. Wu, J. Hu, W. Liu, Y. Zhang, Y. Yang, L. Jia, D. Huang, B. Jia, and D. J. Moss, "Silicon photonic waveguide and microring resonator polarizers incorporating 2D graphene oxide films," *Applied Physics Letters,* vol. 125, no. 5, 2024.
161. H. Arianfard, S. Juodkazis, D. J. Moss, and J. Wu, "Sagnac interference in integrated photonics," *Applied Physics Reviews,* vol. 10, no. 1, 2023.
162. D. Jin, S. Ren, J. Hu, D. Huang, D. J. Moss, and J. Wu, "Modeling of Complex Integrated Photonic Resonators Using the Scattering Matrix Method," *Photonics,* vol. 11, no. 12, pp. 1107, 2024.
163. J. Wu, Y. Yang, Y. Qu, X. Xu, Y. Liang, S. T. Chu, B. E. Little, R. Morandotti, B. Jia, and D. J. Moss, "Graphene Oxide Waveguide and Micro-Ring Resonator Polarizers," *Laser & Photonics Reviews,* vol. 13, no. 9, pp. 1900056, 2019.

 doi:10.20944/preprints202505.2452.v1




164. J. Hu, J. Wu, D. Jin, S. T. Chu, B. E. Little, D. Huang, R. Morandotti, and D. J. Moss, "Thermo-Optic Response and Optical Bistablility of Integrated High-Index Doped Silica Ring Resonators," *Sensors*, vol. 23, no. 24, pp. 9767, 2023.
165. Yunyi Yang, Jiayang Wu, Xingyuan Xu, Sai T. Chu, Brent E. Little, Roberto Morandotti, Baohua Jia, and David J. Moss, "Enhanced four-wave mixing in graphene oxide coated waveguides", Applied Physics Letters Photonics vol. 3 120803 (2018). doi: 10.1063/1.5045509.
166. Wu, J. et al., "Graphene oxide waveguide and micro-ring resonator polarizers", Laser and Photonics Reviews Vol. 13, 1900056 (2019).
167. Jiayang Wu, Yunyi Yang, Yang Qu, Xingyuan Xu, Yao Liang, Sai T. Chu, Brent E. Little, Roberto Morandotti, Baohua Jia, and David J. Moss, "Graphene oxide waveguide polarizers and polarization selective micro-ring resonators", Laser and Photonics Reviews vol. 13 (9) 1900056 (2019). DOI:10.1002/lpor.201900056.
168. Wu, J. et al. "2D layered graphene oxide films integrated with micro-ring resonators for enhanced nonlinear optics", Small Vol. 16, 1906563 (2020).
169. Yang Qu, Jiayang Wu, Yunyi Yang, Yuning Zhang, Yao Liang, Houssein El Dirani, Romain Crochemore, Pierre Demongodin, Corrado Sciancalepore, Christian Grillet, Christelle Monat, Baohua Jia, and David J. Moss, "Enhanced nonlinear four-wave mixing in silicon nitride waveguides integrated with 2D layered graphene oxide films", Advanced Optical Materials vol. 8 (21) 2001048 (2020). DOI: 10.1002/adom.202001048. arXiv:2006.14944.
170. Jiayang Wu, Yunyi Yang, Yang Qu, Yuning Zhang, Linnan Jia, Xingyuan Xu, Sai T. Chu, Brent E. Little, Roberto Morandotti, Baohua Jia, and David J. Moss, "Enhanced nonlinear four-wave mixing in microring resonators integrated with layered graphene oxide films", Small vol. 16 (16) 1906563 (2020). DOI: 10.1002/smll.201906563
171. Jiayang Wu, Yunyi Yang, Yang Qu, Xingyuan Xu, Yao Liang, Sai T. Chu, Brent E. Little, Roberto Morandotti, Baohua Jia, and David J. Moss, "Graphene oxide waveguide polarizers and polarization selective micro-ring resonators", Paper 11282-29, SPIE Photonics West, San Francisco, CA, 4 - 7 February (2020). doi: 10.1117/12.2544584
172. Yuning Zhang, Jiayang Wu, Yang Qu, Linnan Jia, Baohua Jia, and David J. Moss, "Design and optimization of four-wave mixing in microring resonators integrated with 2D graphene oxide films", Journal of Lightwave Technology Vol. 39 (20) 6553-6562 (2021). DOI:10.1109/JLT.2021.3101292.
173. Yang Qu, Jiayang Wu, Yuning Zhang, Yao Liang, Baohua Jia, and David J. Moss, "Analysis of four-wave mixing in silicon nitride waveguides integrated with 2D layered graphene oxide films", Journal of Lightwave Technology Vol. 39 (9) 2902-2910 (2021). DOI: 10.1109/JLT.2021.3059721.
174. Y. Qu, J. Wu, Y. Zhang, L. Jia, Y. Yang, X. Xu, S. T. Chu, B. E. Little, R. Morandotti, B. Jia, and D. J. Moss, "Graphene oxide for enhanced optical nonlinear performance in CMOS compatible integrated devices", Paper No. 11688-30, PW21O-OE109-36, 2D Photonic Materials and Devices IV, SPIE Photonics West, San Francisco CA March 6-11 (2021). doi.org/10.1117/12.2583978
175. Yuning Zhang, Jiayang Wu, Yang Qu, Linnan Jia, Baohua Jia, and David J. Moss, "Optimizing the Kerr nonlinear optical performance of silicon waveguides integrated with 2D graphene oxide films", Journal of Lightwave Technology Vol. 39 (14) 4671-4683 (2021). DOI: 10.1109/JLT.2021.3069733.
176. Yang Qu, Jiayang Wu, Yuning Zhang, Yunyi Yang, Linnan Jia, Baohua Jia, and David J. Moss, "Photo thermal tuning in GO-coated integrated waveguides", Micromachines Vol. 13 1194 (2022). doi.org/10.3390/mi13081194
177. Zhang Y, Wu J, Qu Y, Jia L, Jia B, D.J. Moss, "Graphene oxide-based waveguides for enhanced self-phase modulation", Annals of Mathematics and Physics Vol. 5 (2) 103-106 (2022). DOI:10.17352/amp.000048
178. Yuning Zhang, Jiayang Wu, Yunyi Yang, Yang Qu, Linnan Jia, Baohua Jia, and David J. Moss, "Enhanced spectral broadening of femtosecond optical pulses in silicon nanowires integrated with 2D graphene oxide films", Micromachines Vol. 13 756 (2022). DOI:10.3390/mi13050756.
179. Yuning Zhang, Jiayang Wu, Yunyi Yang, Yang Qu, Linnan Jia, Houssein El Dirani, Sébastien Kerdiles, Corrado Sciancalepore, Pierre Demongodin, Christian Grillet, Christelle Monat, Baohua Jia, and David J.

 doi:10.20944/preprints202505.2452.v1



Moss, "Enhanced supercontinuum generated in SiN waveguides coated with GO films", ***Advanced Materials Technologies*** **8** (1) 2201796 (2023). DOI:10.1002/admt.202201796.

180. Yuning Zhang, Jiayang Wu, Yunyi Yang, Yang Qu, Houssein El Dirani, Romain Crochemore, Corrado Sciancalepore, Pierre Demongodin, Christian Grillet, Christelle Monat, Baohua Jia, and David J. Moss, "Enhanced self-phase modulation in silicon nitride waveguides integrated with 2D graphene oxide films", IEEE Journal of Selected Topics in Quantum Electronics Vol. 29 (1) 5100413 (2023). DOI: 10.1109/JSTQE.2022.3177385
181. Yang Qu, Jiayang Wu, Yuning Zhang, Yunyi Yang, Linnan Jia, Houssein El Dirani, Sébastien Kerdiles, Corrado Sciancalepore, Pierre Demongodin, Christian Grillet, Christelle Monat, Baohua Jia, and David J. Moss, "Integrated optical parametric amplifiers in silicon nitride waveguides incorporated with 2D graphene oxide films", ***Light: Advanced Manufacturing*** **4** 39 (2023). https://doi.org/10.37188/lam.2023.039.
182. Jiayang Wu, Yuning Zhang, Junkai Hu, Yunyi Yang, Di Jin, Wenbo Liu, Duan Huang, Baohua Jia, David J. Moss, "Novel functionality with 2D graphene oxide films integrated on silicon photonic chips", ***Advanced Materials*** Vol. 36 2403659 (2024). DOI: 10.1002/adma.202403659.
183. Di Jin, Jiayang Wu, Junkai Hu, Wenbo Liu, Yuning Zhang, Yunyi Yang, Linnan Jia, Duan Huang, Baohua Jia, and David J. Moss, "Silicon photonic waveguide and microring resonator polarizers incorporating 2D graphene oxide films", Applied Physics Letters, Vol. 125, 053101 (2024). doi: 10.1063/5.0221793.
184. Yuning Zhang, Jiayang Wu, Linnan Jia, Di Jin, Baohua Jia, Xiaoyong Hu, David Moss, Qihuang Gong, "Advanced optical polarizers based on 2D materials", ***npj Nanophotonics*** **1**, 28 (2024). DOI: 10.1038/s44310-024-00028-3.
185. Y. Zhang, J. Wu, Y. Yang,Y. Qu, L. Jia, C. Grillet, C. Monat, B. Jia, and D.J. Moss, "Graphene oxide for enhanced nonlinear optics in integrated photonic chips", Paper 12888-16, Conference OE109, 2D Photonic Materials and Devices VII, Chair(s): Arka Majmdar; Carlos M. Torres Jr.; Hui Deng, SPIE Photonics West, San Francisco CA, January 27 – February 1 (2024). Proceedings Volume 12888, 2D Photonic Materials and Devices VII; 1288805 (2024). https://doi.org/10.1117/12.3005069
186. Di Jin, Wenbo Liu, Linnan Jia, Junkai Hu, Duan Huang, Jiayang Wu, Baohua Jia, and David J. Moss, "Thickness and Wavelength Dependent Nonlinear Optical Absorption in 2D Layered MXene Films", ***Small Science*** **4** 2400179 (2024). DOI:10.1002/smsc202400179;
187. Yuning Zhang, Jiayang Wu, Junkai Hu, Linnan Jia, Di Jin, Baohua Jia, Xiaoyong Hu, David J. Moss, Qihuang Gong, "2D material integrated photonics: towards industrial manufacturing and commercialization", Applied Physics Letters Photonics **10**, 000000 (2025); doi: 10.1063/5.0249703.
188. Linnan Jia, Yang Qu, Jiayang Wu, Yuning Zhang, Yunyi Yang, Baohua Jia, and David J. Moss, "Third-order optical nonlinearities of 2D materials at telecommunications wavelengths", ***Micromachines***, **14** 307 (2023). https://doi.org/10.3390/mi14020307.
189. Linnan Jia, Jiayang Wu, Yuning Zhang, Yang Qu, Baohua Jia, Zhigang Chen, and David J. Moss, "Fabrication Technologies for the On-Chip Integration of 2D Materials", Small: Methods Vol. 6, 2101435 (2022). DOI:10.1002/smtd.202101435.
190. Linnan Jia, Dandan Cui, Jiayang Wu, Haifeng Feng, Tieshan Yang, Yunyi Yang, Yi Du, Weichang Hao, Baohua Jia, David J. Moss, "BiOBr nanoflakes with strong nonlinear optical properties towards hybrid integrated photonic devices", Applied Physics Letters Photonics vol. 4 090802 vol. (2019). DOI: 10.1063/1.5116621
191. Linnan Jia, Jiayang Wu, Yunyi Yang, Yi Du, Baohua Jia, David J. Moss, "Large Third-Order Optical Kerr Nonlinearity in Nanometer-Thick PdSe2 2D Dichalcogenide Films: Implications for Nonlinear Photonic Devices", ACS Applied Nano Materials vol. 3 (7) 6876–6883 (2020). DOI:10.1021/acsanm.0c01239.
192. Kues, M. et al. "Quantum optical microcombs", Nature Photonics vol. 13, (3) 170-179 (2019). doi:10.1038/s41566-019-0363-0
193. C.Reimer, L. Caspani, M. Clerici, et al., "Integrated frequency comb source of heralded single photons," Optics Express, vol. 22, no. 6, pp. 6535-6546, 2014.
194. C. Reimer, et al., "Cross-polarized photon-pair generation and bi-chromatically pumped optical parametric oscillation on a chip", Nature Communications, vol. 6, Article 8236, 2015. DOI: 10.1038/ncomms9236.

 doi:10.20944/preprints202505.2452.v1




195. L. Caspani, C. Reimer, M. Kues, et al., "Multifrequency sources of quantum correlated photon pairs on-chip: a path toward integrated Quantum Frequency Combs," Nanophotonics, vol. 5, no. 2, pp. 351-362, 2016.
196. C. Reimer et al., "Generation of multiphoton entangled quantum states by means of integrated frequency combs," Science, vol. 351, no. 6278, pp. 1176-1180, 2016.
197. M. Kues, et al., "On-chip generation of high-dimensional entangled quantum states and their coherent control", Nature, vol. 546, no. 7660, pp. 622-626, 2017.
198. P. Roztocki et al., "Practical system for the generation of pulsed quantum frequency combs," Optics Express, vol. 25, no. 16, pp. 18940-18949, 2017.
199. Y. Zhang, et al., "Induced photon correlations through superposition of two four-wave mixing processes in integrated cavities", Laser and Photonics Reviews, vol. 14, no. 7, pp. 2000128, 2020. DOI: 10.1002/lpor.202000128
200. C. Reimer, et al., "High-dimensional one-way quantum processing implemented on d-level cluster states", Nature Physics, vol. 15, no.2, pp. 148–153, 2019.
201. P.Roztocki et al., "Complex quantum state generation and coherent control based on integrated frequency combs", Journal of Lightwave Technology vol. 37 (2) 338-347 (2019).
202. S. Sciara et al., "Generation and Processing of Complex Photon States with Quantum Frequency Combs", IEEE Photonics Technology Letters vol. 31 (23) 1862-1865 (2019). DOI: 10.1109/LPT.2019.2944564.
203. Nicola Montaut, Agnes George, Monika Monika, Farzam Nosrati, Hao Yu, Stefania Sciara, Benjamin Crockett, Ulf Peschel, Zhiming Wang, Rosario lo Franco, Mario Chemnitz, William J. Munro, David J. Moss, José Azaña, and Roberto Morandotti, "Progress in integrated and fiber optics for time-bin based quantum information processing", Advanced Optical Technologies **14** 1560084 (2025).
a. DOI 10.3389/aot.2025.1560084
204. Hao Yu, Benjamin Crockett, Nicola Montaut, Stefania Sciara, Mario Chemnitz, Sai T Chu, Brent E Little, David J Moss, Zhiming Wang, José Azaña, And Roberto Morandotti, "Exploiting nonlocal correlations for dispersion-resilient quantum communications", ***Physical Review Letters* 134** (2025).
205. Stefania Sciara, Piotr Roztocki, Bennet Fisher, Christian Reimer, Luis Romero Cortez, William J. Munro, David J. Moss, Alfonso C. Cino, Lucia Caspani, Michael Kues, J. Azana, and Roberto Morandotti, "Scalable and effective multilevel entangled photon states: A promising tool to boost quantum technologies", Nanophotonics vol. 10 (18), 4447–4465 (2021). DOI:10.1515/nanoph-2021-0510.
206. L. Caspani, C. Reimer, M. Kues, et al., "Multifrequency sources of quantum correlated photon pairs on-chip: a path toward integrated Quantum Frequency Combs," Nanophotonics, vol. 5, no. 2, pp. 351-362, 2016.
207. H. Yu, S. Sciara, M. Chemnitz, N. Montaut, B. Fischer, R. Helsten, B. Crockett, B. Wetzel, T. A. Göbel, R. Krämer, B. E. Little, S. T. Chu, D. J. Moss, S. Nolte, W.J. Munro, Z. Wang, J. Azaña, R. Morandotti, "Quantum key distribution implemented with d-level time-bin entangled photons", ***Nature Communications* 16** 171 (2025). DOI:10.1038/s41467-024-55345-0.